Intracontinental orogenesis in the heart of Australia: Structure, provenance and tectonic significance of the Bentley Supergroup, Western Musgrave Block, Western Australia

Peter Coleman

Tectonics, Resources and Exploration
Discipline of Geology and Geophysics
School of Earth and Environmental Sciences
University of Adelaide, South Australia
peter.coleman@student.adelaide.edu.au

Table of Contents

Intracontinental orogenesis in the heart of Australia: Structure, provenance and tectonic significance of the Bentley Supergroup, Western Musgrave Block, Western Australia

Peter Coleman

Tectonics, Resources and Exploration
Discipline of Geology and Geophysics
School of Earth and Environmental Sciences
University of Adelaide, South Australia
peter.coleman@student.adelaide.edu.au

Abstract

Volcanic rocks attributed to the ca. 1080 Ma Giles Event were extruded within the western Musgrave Block in the late Mesoproterozoic. SHRIMP U-Pb analysis of 2 samples of zircon cores from rhyolites approximately 2km SSE of Blackstone Range yielded $^{238}U/^{206}Pb$ crystallisation ages of 1071±8 Ma and 1073± 7 Ma. These rhyolites, forming the base of the Smoke Hill Volcanics at Mount Jane, were unconformably emplaced over the Blackstone Range layered intrusions in a series of separate flows. Soon after being extruded the rhyolites were deformed and developed pervasive NE-or SW dipping foliation within a 2km wide shear zone at Mount Jane. Garnet and epidote replacement of plagioclase phenocrysts indicate at least lower amphibolite-facies metamorphism was attained within the near vertical, south-dipping ultramylonite centre of the shear zone. Shear sense indicators within the shear zone almost exclusively give north side down kinematics in outcrop and in thin section. A syn-tectonic micro-granite intrudes the centre of the shear zone with veins that cross-cut the ultramylonitic foliation and hence post dates shearing. This micro-granite yields a $^{238}U/^{206}Pb$ vs. $^{207}Pb/^{206}Pb$ isotope ratio zircon age of 1070±5 Ma. Thin, highly luminescent, structureless rims surround the zircons, and yield a similar or slightly younger age than the cores. Therefore the deformation was most likely synchronous, or soon after, the eruption of the rhyolite as part of the Giles Event. A series of mafic and intermediate volcanic rocks attributed to the Hogarth Formation directly overlie the rhyolite, which steeply dip towards the south and have been cut by a series of later stage gabbros and granites.

Keywords: Musgrave Block, Giles Event, Tollu Group, volcanics, deformation, zircon

1. Introduction

A number of deformational, metamorphic and magmatic events are preserved within Musgrave Block, Central Australia, ranging from early Mesoproterozoic to the late Neoproterozoic. The first known deformational and magmatic event, restricted to the West Musgrave Block was the 1336-1293 Ma Mount West Orogeny (Howard et al., 2007), during which the Wankanki Supersuite granites and Wirku Metamorphics were formed. Early structural fabrics formed during the Mount West Orogeny were overprinted and deformed during the 1219-1155 Ma Musgravian Orogeny (Smithies et al., 2009a). This high grade deformational event produced widespread amphibolite to granulite reworking and associated magmatism known as the Pitjantjatjara Supersuite granite, which forms a large proportion of out crop within the Musgrave Block (Figure 1a) (Clarke et al. 1995; Edgoose et al., 2004).

The ca. 630-520 Ma Petermann Orogeny was a transpressional event which exhumed the Musgrave Block from beneath the once contiguous Centralian Superbasin (Hand and Sandiford 1999, Wade et al., 2008). Structures formed in the Mesoproterozoic were re-activated, overprinting much evidence of earlier deformation during the high grade Neoproterozoic event (Camacho and Fanning, 1995). Deformation was focused along a series of east-west trending fault structures namely the Hinckley, Mann and Woodroffe Thrusts (Camacho et al., 1997; Sandiford et al., 2001). These faults penetrated the deep crust. Detailed studies of mineral assemblages within the shear zone have provided strong evidence of high-pressure metamorphism (11-14 kbar and 700ºC) and therefore estimate exhumation in the order of up to 40km (Camacho, 1997, Clarke et al., 1995 and Scrimgeour & Close, 1999). In the Western Musgrave Block, the region north of the Mann Fault was extruded northwards in a recently proposed crustal-scale channel during the Petermann Orogeny (Raimondo et al., 2009).

The Bentley Supergroup is a package of mafic and felsic volcanic rocks which were extruded in the West Musgrave Block during the ca. 1080 Ma Giles Event (Clarke et al., 1995; Glikson et al., 1996). These mafic and felsic volcanics, together with the mafic-ultramafic layered intrusions (Giles Complex), gabbros, granites and mafic dykes form the Warakurna Supersuite, best exposed in the Western Musgrave Block. Mafic dykes geochemically and geochronologically correlated with the layered mafic-ultramafic intrusions crop out across approximately 1.5 million km², from central Australia to far west Western Australia, forming the Warakurna Large Igneous Province (LIP) (Wingate et al., 2004; Morris and Pirajno, 2005). Since their emplacement, the layered igneous rocks of the Giles Complex have been macroscopically folded and deformed (Smithies et al., 2009a). 1075±7 Ma Giles Event granite dykes cross-cut the folded intrusions, providing a minimum age of their emplacement and evidence of at least some deformation (D3) during the magmatic event (Kirkland et al., 2008b). Bi-modal volcanic rocks of the Tollu Group, Bentley Supergroup, found in the core of the Tollu basin of the BLACKSTONE 1:100 000 map sheet (Smithies et al., 2009b) overlie the deformed layered intrusions. These volcanics are believed to also be macroscopically folded about the same axis as the layered mafic-ultramafic rocks (Smithies et al., 2009b; Evins et al.,

in press), suggesting that the co-magmatic deformation persisted during their extrusion. Alternatively it's possible that the layers of the Tollu Group may have slumped into a previously formed topographic basin (Evins et al., in press). Despite the extensive outcrop of the Warakurna Supersuite rocks within central Australia, the age and deformational history of the Giles Event is still poorly constrained. The origin of the Warakurna LIP is also uncertain, with some workers suggesting a mantle plume (Morris and Pirajno, 2005), whilst more recently, Evins et al. (in press) suggest a long-lived intracontinental rift system, named the Ngaanyatjarra Rift as the likely source of magmatism and deformation.

Little work has been conducted on the Warakurna Supersuite, and many of the geochronological and structural studies of the Mesoproterozoic Giles Event have focused on the mafic-ultramafic layered intrusions, due to their large size, exposure and their significant economic potential for Ni-Cu and PGE mineralisation. As a result less attention has been directed towards the associated, bi-modal Bentley Supergroup. This study presents field relationships and structural mapping, U-Pb zircon Sensitive High Resolution Ion-Microprobe (SHRIMP) dating and optical microscopic strain analysis in an attempt to investigate and better understand the depositional, structural, kinematic and geochronological record of a deformed region of the Bentley Supergroup, Western Musgrave Block.

2. Geological setting of the Musgrave Block

The Musgrave Block is an early Mesoproterozoic to Neoproterozoic E-W trending basement inlier within central Australia that straddles the South Australian, Western Australian and Northern Territory borders (Figure 1a). It is bound to the north and south by the Neoproterozoic to Palaeozoic Amadeus and Officer Basins respectively, and the Permian to Mesozoic Eromanga Basin to the east. The Proterozoic basement complex spans some 120,000 km² and represents one of the largest intracontinental geophysical anomalies in the world (Sandiford, 2002).

The Musgrave Block is one of the best exposed and most extensive Proterozoic terrains of Australia, yet is one of the least studied and poorly understood. Although importantly, it lies on the junction between the three Archean cratonic blocks of Australia (North, West and South Australian cratons) and accordingly provides an essential link to the understanding of paleogeographic reconstructions of Proterozoic Australia. The first regional geological studies of the Musgrave Block were undertaken by Sprigg and Wilson (1959). Much of the early studies focused on regional geological mapping and has provided the bulk of our current understanding of the Musgrave Block, with a strong emphasis on the prospective Giles layered intrusions (eg. Nesbitt and Kleeman, 1964; Goode, 1970; Moore, 1970; Collerson, 1972; Daniels, 1974; Thompson, 1975). Early geochronological studies, utilising the Rb-Sr system were mostly conducted by Gray (1977, 1978). This early work allowed for the recognition and sub-division of the Musgrave Block into the mostly amphibolite facies Mulga Park Domain to the north of

the large scale south-dipping Woodroffe Thrust, and the dominantly granulite facies Fregon Domain to the south.

The oldest known exposed rocks within the Musgrave Block are gneisses that were deposited between 1600-1540 Ma (Smithies et al., 2009a) with volcanic, volcaniclastic and sedimentary origins (Major and Conner, 1993; Camacho and Fanning, 1995; Edgoose et al., 2004). These supracrustal Mesoproterozoic rocks are grouped into the Birksgate Complex and coupled with the 1220-1140 Ma Pitjantjatjara Supersuite granites form a majority of the exposed rocks within the Musgrave Block (Smithies et al., 2009a; Wade et al., 2008). Geochemical and isotopic studies by Wade et al. (2006) concluded that the dominantly felsic Birksgate Complex had affinities with island-arc subduction setting volcanism and likely formed during an earlier stage of cratonic convergence between the north and south Australian cratons. Voluminous felsic intrusive magmatism intruded the basement lithologies between 1336-1293 Ma (Wankaki Supersuite) with associated granulite facies metamorphism and migmatisation development (Sun and Sheraton, 1992). This magmatic event was believed to be restricted to the Western Musgrave Block, contemporaneous with the first recorded period of deformation and associated development of structural fabrics (D1) (White et al., 1999; Wade et al., 2008). This early deformational event has recently been named the Mount West Orogeny (Howard et al., 2007) and correlations of such with that of the Albany-Fraser, further to the south, has led some authors to suggest a shared tectonic history (Clark et al., 2000).

The 1220-1150 Ma Musgrave Orogeny (D2) was the oldest orogenic event to have clearly affected all areas of the Musgrave Block with peak metamorphic conditions reaching in excess of 800ºC and 5 kbar (Clarke et al., 1995). This high grade event largely destroyed structural fabrics formed during the earlier Mount West Orogeny (Howard et al., 2007; Smithies et al., 2009a) and produced zircon overgrowths with U-Pb dates of ~1200 Ma (White et al. 1999). Widespread granite emplacement, synchronous in age with the Musgravian Orogeny, (the Pitjantjatjara Supersuite) range from diorite to monzonite in composition and have within plate, A-type affinities (Smithies et al., 2009a). These form the majority of outcrop of the Musgrave Block, particularly within the Mulga Park Domain (Wade et al., 2008). The Musgrave and Mount West orogenies together, are correlated with and provide a link between the Musgrave Block and the Albany-Fraser Complex along the south-western margin of Australia and continues into the Bunger Hills and Windmill Islands regions of Antarctica. This widespread orogeny is thought to represent the final amalgamation of cratonic Australia during the assembly of Rodinia (Myers et al., 1996; Fitzsimons, 2003).

Following D2, was a second major phase of magmatism within the Musgrave Block, with large-scale emplacement of layered mafic-ultramafic intrusions into the high-grade terrain. The age of the layered Giles intrusions is poorly constrained with a minimum U-Pb SHRIMP emplacement age of 1078±3 Ma for a granophyric leucogranite that truncates the layering at Bell Rock. The maximum age constraint on the layered intrusions is a latest Musgravian Orogeny age of c. 1170 Ma. All igneous rocks related to the ca. 1080 Ma Giles Event in the West Musgrave Block are grouped into the 'Warakurna Supersuite' and include the massive to variably deformed layered mafic-

ultramafic Giles Complex, granitic and gabbroic intrusions, mafic dykes and bi-modal volcanics of the Bentley Supergroup. Coeval mafic igneous rocks of the Warakurna Supersuite were emplaced over 1.5 million km² of central to far west Western Australia and the erosional remnants of which represent the Warakurna Large Igneous Province (Wingate et al., 2004; Morris and Pirajno, 2005). The sheer size and nature of the layered intrusions and associated volcanics, best exposed in the West Musgrave Block has led some authors to suggest a mantle plume as the likely source of magmatism (Wingate et al., 2004; Morris and Pirajno, 2005). More recent detailed studies by Evins et al. (in press) has argued that sporadic continuation of igneous activity and associated deformation for over 50 Ma to ca. 1026 Ma (Edgoose et al., 2004), requires a geodynamic setting more complex than a single mantle plume head, more akin to that of a long-lived failed rift system.

Bimodal volcanic and interlayered sedimentary rocks of the Tollu Group, Bentley Supergroup were thought to be synchronous in age with the layered Giles intrusions based on a 1075±5 Ma age (Glikson et al., 1996; Edgoose et al., 2004). More recently, Smithies et al. (2009a) have argued that the dated outcrop was not a volcanic rock, but part of the older leucogranite suite related to the Giles event and that the Tollu Group formed a short period after the Giles Complex. The Tjauwata Group in Northern Territory is a package of deformed sediments and bi-modal volcanics that crop out between the Petermann and Bloods Ranges, north of the Woodroffe Thrust (Figure 1a) and consist of basal quartzite and conglomerate, basalt overlain by rhyolites and epiclastic sediments. The Tjauwata Group is considered a correlative of the Bentley Supergroup volcanics and associated sediments that comprise the south-west Musgrave Block (Glikson et al., 1996; Edgoose et al., 2004). The Mount Harris Basalt of the Tjauwata Group (correlative of the Mummawarrawarra Basalt, Bentley Supergroup) is intruded by the Walu Granite which yields a SHRIMP U-Pb zircon age of 1084±9 Ma. The minimum age of volcanism is obtained from the Wankari Volcanics (correlative of the Hogarth Formation, Tollu Group), yielding a ^{207}Pb-^{206}Pb age of 1041±2 Ma (Close et al., 2003; Edgoose et al., 2004; Wade et al., 2008).

The layered Giles Intrusions in the Jameson area of the south-west Musgrave Block alone preserve an exposed thickness of 10km, but Smithies et al. (2009a) suggest that it is likely that the troctolitic Bell Rock, Blackstone, and Jameson-Finlay intrusions are tectonically dislocated parts of a single intrusion and therefore could possibly have been up to 170km long, 25km wide and 10km thick. Massive gabbros and syn-mylonitic leucogranites intrude and locally engulf the layered mafic-ultramafic intrusions. In a northwest-trending mylonite immediately south of Charnockite Flats, south-west Musgrave Block, are leucogranite dykes that intrude as boudin necks. U-Pb SHRIMP dating of these leucogranite intrusions yields an age of 1075±2 Ma (Kirkland et al., 2008a), thus effectively gives evidence of multi-phase intrusions of magma and deformation during the Giles Event (Smithies et al., 2009a; Evins et al., in press). This deformational event (D3) is responsible for much of the near vertical foliation and tight to isoclinal folds with axial planar, steep southerly-dipping mylonitic shear zones throughout much of the western Musgrave Block (Glikson et al., 1996; White et al., 1999). Evins et al. (in press) has argued that there must exist up to at least 10 episodes of magmatism accompanied by

intense deformation over at least 50 m.y. Coeval with the Giles Event was the widespread emplacement of mafic dykes, thought to be feeder dykes to the large-scale Giles Complex. These dykes crop out as far as the western margin of Australia and are contemporaneous with the ~1070 Ma Alcurra and Stuart Pass Dolerite in Northern Territory. A series of younger mafic dykes post-date the Giles Event and crop out extensively throughout the Musgrave Block. These include the ~1000 Ma Kullal dykes and the ~820 Ma Gairdner and Amata dyke swarm which have been linked on the basis of their similar ages and chemistry (Glikson et al., 1996) and thought to represent a period of extension associated with the breakup of Rodinia (Cawood, 2005).

After nearly a 400 m.y hiatus in any significant deformation, the Musgrave Block was exhumed from beneath, and divided, the Centralian Superbasin in the late Neoproterozoic Petermann Orogeny (Cawood and Korsch, 2008). Sm-Nd-isotopic and geochemical studies from within the Officer Basin indicate a large influx of Musgrave-Block derived sediments at ~600 Ma and is interpreted to represent the un-roofing and initiation of the Petermann Orogeny (Wade et al., 2005). The Petermann Orogeny was a widespread, high-grade event which focused deformation along deep-penetrating E-W trending Mesoproterozoic structures (e.g. Woodroffe Thrust and Mann Fault). Substantial crustal thickening occurred along these structures (Flöttmann et al., 2004) and caused juxtaposition of higher grade granulite facies gneisses from depths of 40-45km, south of the Woodroffe Thrust with amphibolite facies Mulga Park Domain to the north (Scrimgeour and Close, 1999). Deformation was centered on the northern part of the Musgrave Block, in the vicinity of the Woodroffe-Mann Thrust fault systems (Hand and Sandiford 1999), with north-directed thrusting of the Fregon Domain over the Mulga Park Domain and south-directed thrusting of the Fregon Domain over the Officer Basin in the south, characteristic of a positive flower structure (Hand and Sandiford 1999; Camacho and McDougall, 2000). Recent structural, metamorphic and geochronological studies by Raimondo et al. (2009) has proposed that intracontinental channel flow north of the Mann Fault was active during the Petermann Orogeny. These studies indicate that the deeply exhumed orogenic core is bound by thrust and normal-sense shear zones on its northern and southern margins respectively, and coupled with the gravitational loading of the orogen by thrust-assisted crustal thickening was sufficient to generate the lateral lithostatic pressure gradient necessary to drive lower-crustal flow (Raimondo et al., 2009). Deformation during Petermann Orogeny has controlled the currently exposed outcrop pattern within the Musgrave Block with the last known period of exhumation preserved by synkinematic biotite and muscovite growth within the Woodroffe Thrust dated at 520 Ma (Camacho and Fanning, 1995). The Petermann Orogen is typically considered as a dextral transpressive shear system, likely to be the result of north-south directed compression of the Australian plate during amalgamation of Gondwana in the Neoproterozoic (Sandiford and Hand, 1998; Collins and Pisarevsky, 2005). Many authors, based on similarities in age and nature, have correlated the Petermann Orogeny to the intracratonic 550 Ma Paterson Orogeny, further to the northwest (Edgoose et al., 2004).

3. Structural setting and field relationships

Field work for this study was undertaken in the north-eastern portion of Geological Survey of Western Australia's (GSWA) newly released BLACKSTONE 1:100 000 Map sheet (Figure 1b) (Smithies et al., 2009b). Detailed 1:10 000 scale mapping was undertaken both within a highly deformed and sheared region of the Tollu Group rhyolite at Mount Jane and secondly, approximately 15km to the west, on a relatively less deformed stratigraphic succession through the Tollu Group and Hogarth Formation at Barnard Rocks (Figure 1b). Geological maps and structural cross-sections were constructed through these two terrains and presented in Figures 2-5. Further study was conducted 1-2 km's north and south of the Mount Jane shear zone to investigate the lithological and structural variation across strike.

3.1. Lithology

A fairly homogenous lithological framework exists at Mount Jane. The rocks are broadly characterised by porphyritic rhyolite as a lava with up to 10-15%, 1-6mm sized phenocrysts of microcline and plagioclase in a finer-grained aphanitic, grey coloured, <0.3mm quartz and hornblende, and to a lesser degree biotite, dominated matrix. Indications of surficial flow are present with igneous flow banding and flow folds (Figure 6a). Subtle variations across strike, however, in the grain size and composition of the matrix and abundance of phenocrysts within the rhyolite, suggest that the rhyolite formed from a series of separate flows, 10's to 100's of meters thick. Broadly, these variations include very fine-grained and phenocryst-free rhyolites with a conchoidal fracture north of Mount Jane, quartz-dominated rhyolites in the centre of Mount Jane, and coarser-grained almost sub-volcanic rhyolites to the south. Most variations in rock type observed at Mount Jane are a function of the amount of strain. The rocks have been moderately to strongly deformed within a large (at least 2km wide) ESE-trending shear zone, with up to ultramylonite rhyolite preserved between Mount Jane and Mount Maria (centre of shear zone, Figure 2) grading into mylonite and strongly foliated rhyolite respectively, away from the centre of the shear zone (Figure 2).

There are two strikingly different lithologies adjacent the ultramylonite zone (Figure 2), 1) a meta-andesite and 2) a brecciated rhyolite flow with jigsaw fit texture (Figure 6d). The meta-andesite unit is more thoroughly described in section 4.4 below, but is hornblende-dominated and has a variable thickness and departure along strike (thus likely represents a lens). Stratigraphically below this unit is an abrupt change to a jigsaw-fit rhyolite breccia lens (Figure 2) with fragments ranging from 30cm to 1mm, held together by a pale siliceous matrix. This 20-50m thick unit also contains abundant 2-10mm spherulites and 2-30mm quartz filled amygdales. This breccia is interpreted to have formed by rapid cooling of the volcanic flow and brecciation by interaction of a water saturated body to form a hyaloclastite. Interestingly, however, this unit is not foliated nearly as much as it's stratigraphically higher and lower neighbours, possibly as a result of strain partitioning within the WNW trending shear zone.

In the middle of the ultramylonite zone lies a micro-granite intrusive body (Figure 2, 3). The holocrystalline granite is fine-grained (<3mm) and pale coloured with a felsic mineralogy consisting of 1-2mm K-feldpar and plagioclase crystals, slightly larger quartz crystals and only minor amounts of mafic minerals in the form of ~5% biotite and/or hornblende.. The microgranite pluton is completely undeformed in its centre (sample 191716, Figure 2), but on its margins it is strongly foliated in the same orientation as the adjacent ultramylonitic rhyolite. The ultramylonitic fabric surrounds and wraps around the intrusive pluton, which is interpreted to act as an obstacle to shearing. In close proximity to the intrusive granite are veins of similar lithology (which were not observed elsewhere), which cross-cut the deformational fabric (Figure 7b). These granite dykes are correlated with the larger body. The observation that the micro-granite intrusion appears to be affected by the mylonitic strain in some places, yet cross-cuts the mylonitic fabric in other places, thus leads to an interpretation of a syn-deformational intrusion.

Approximately 100m south of the Mount Jane shear zone are sporadic, poorly foliated, aphanitic textured amygdaloidal basalts (Figure 2). Mafic rocks with 2-3mm opx, cpx and plagioclase are preserved within the basalt, possibly as later stage intrusions. This unit strongly resembles other amygdaloidal basalts seen elsewhere within the BLACKSTONE map sheet which the GSWA have mapped as the basal unit of the Hogarth Formation, which stratigraphically overlies the rhyolites of the Smoke Hill Volcanics (Smithies et al., 2009b). In the section drawn through Mount Jane (Figure 3), these amygdaloidal basalts lie stratigraphically beneath the rhyolite, but a detailed transect a further 900m to the south west through the equivalent contact of the rhyolite and amygdaloidal basalt indicates that the amygdaloidal basalt directly overlies the rhyolite. Therefore, it's possible that the volcanics at, and directly south of Mount Jane have been folded and overturned and likewise the amygdaloidal basalt overlies the rhyolite, or alternatively there is a separate amygdaloidal basalt unit beneath the rhyolite at Mount Jane. Igneous layering (Figure 6c) within the basalt, south west of Mount Jane dips moderately to the south (35/191), indicating at least some macroscopic folding between the two locations.

The contact between the Smoke Hill Volcanics and the underlying layered mafic intrusions of the Blackstone Range is rarely observed due to weathering and poor exposure. The northern-most exposed volcanics, north Mount Jane are separated by no more than 750m of magnetite-rich cover from the southeastern-most exposed outcrop of the Giles Complex layered intrusion of Blackstone Range. Adjacent to, and hugging the northern tip of the exposed volcanics, lies a much more mafic, dense, magnetic and dark-coloured rock (Figure 6b). This holocrystalline rock has a mineralogy dominated by 1-3mm pyroxene, some plagioclase and possibly amphibole. This gabbro/pyroxenite preserves a moderate foliation (Figure 6b) at an oblique angle (~65/094) (therefore pre-dates Mount Jane shear zone) to the E-W trending, overlying rhyolite foliation. Although the exact contact between these two units is obscured by weathering (Figure 6b), the gabbro/pyroxenite is not observed cross cutting the rhyolite and due to the dissimilar nature of the foliation between the two units; it is possible that the gabbro represents part of the Blackstone Range intrusives, which the rhyolite has been unconformably extruded above.

The Barnard Rocks area is much more lithologically variable than Mount Jane, comprising of a series of E-W trending volcanic packages (Figure 4). These steeply south-dipping volcanic packages include rhyolites, amygdaloidal basalts, volcanic breccias and trachyte/andesites (Figure 4, 5). Upward younging directions were indicated by graded igneous layering within the volcanic breccia (Figure 6f), and although hard to determine, no evidence exists to suggest overturned bedding. The andesite flow in the north of the Barnard Rocks mapping area had overall gradual upwards fining from clearly observed crystals at its base in the north to very fine-grained, glassy textured in the south. The rhyolite unit observed in the north of the mapping area (Figure 4) has a porphyritic, aphanitic texture with 2-3mm plagioclase phenocrysts in a fine-grained, smoky-grey quartz-dominated matrix with common igneous layering and auto-brecciation observed (Figure 6e), indicating flow during extrusion. This rhyolite is strikingly similar to the rhyolite observed at Mount Jane, and also lies on nearly the same northing, thus it is interpreted to represent the same unit within the Tollu Group. This rhyolite forms the stratigraphic base of the upwards younging succession at Barnard Rocks (Figure 5) and is overlain by an amygdaloidal basalt to the south, again appearing similar to that of south Mount Jane. Therefore the Mount Jane/Barnard Rocks regions can provide a nearly complete package through the Tollu Group. A series of later stage ophitic textured-gabbros and coarse-grained syenogranites intrude into the mafic and felsic volcanic sequence and are likely to be equivalent to the elsewhere dated 1075-1060 Ma Giles Event 3 intrusions (Sun et al., 1996; Wingate et al., 2004; Smithies et al., 2009b).

3.2. Structure

The dominant structural element of the Mount Jane region is a pervasive fabric that dips moderate to steeply NE or SW. The intensity and dip of foliation varies spatially, but generally increases towards the NW trending steeply-south-dipping ultramylonite (Figures 2, 3) in the centre of the shear zone. The foliation dips moderately towards the north within the southern outcrops of the foliated rhyolite and progressively becomes steeper to the north until it rotates through the vertical and dips steeply south inside the ultramylonite zone and further to the north (Figure 8b, 2, 3). The intensity of foliation is also variable on the cm to meter scale with boulders appearing nearly unfoliated juxtaposed against rhyolite that encompasses mylonitic foliation (Figure 7a). This strain partitioning was evident in both outcrop and thin-section. The alignment of biotite/hornblende and quartz defines an elongation lineation that dominantly plunges north, at a similar angle to the dip of the foliation planes (Figure 8a).

Shear sense indicators are rare in both outcrop and thin-section, but are locally expressed as rotated phenocrysts of plagioclase (Figure 7c), which consistently give a ‘north-side down’ sense of movement. This north-side down, sense of shear is independent of whether the foliation dipped north or south. A relatively strong correlation exists between topography and degree of strain and aided classification of the shear zone domains outside of the studied area. The zones of least strain and foliation development form the peaks of hills and the ultramylonite zone forms the divide between the peaks of Mount Jane and Mount Maria (Figure 2) and sparsely crops out on the lower flats. The mylonite can be considered as a L-S tectonite with strongly developed foliation and lineation that

likely formed under simple shear. At close proximity to, and within the mylonite and ultramylonite where the level of strain is highest, the lineation is rotated towards the east and west (Figure 2). These highest-strain zones preserve the most convincing evidence for rotational strain (i.e. delta-clasts). Outside of the higher strain zones, the lineation plunges at an angle quite similar to the dip of the foliation (north). The progressive change in orientation of the stretching lineation between high and low strain zones (interpreted to be equivalent to high and low rotational strain) (Figure 2) is interpreted to represent incremental changes in orientation of the principle axis of the finite strain ellipsoid. Therefore under the same bulk N-S directed force, both pure and simple shear strain mechanisms were active within the shear zone causing coaxial and non-coaxial deformation. The higher strained core of the shear zone is affected mostly by simple shear strain, whilst pure shear and coaxial deformation dominates the lower strain zones. The ultramylonite shear zone is characterised by subtle grain size reduction, mica recrystallisation, stronger development of foliation planes (Figure 7d) and elongation of biotite/hornblende and plagioclase phenocrysts (Figure 7e).

Depositional igneous layering that was presumably flat at the time of extrusion has been folded by the deformational event and now mostly dips northwards on the south side of the shear zone and southwards on the north side (Figure 8e). Macroscopic folding of the foliation is best exposed in the far north of Mount Jane where foliation axial planar folds form both tight (5m-scale) and open (100m-scale) folds that plunge moderately towards the west (Figure 8c, d). All the volcanic rocks immediately south of, and including, the Blackstone Range are believed to be preserved within a large-scale structural syncline known as the Blackstone Syncline (Smithies et al., 2009b). The two exposed low hills at Barnard Rocks (Figure 4, 5) supposedly form the northern and southern limbs of this structural syncline (Smithies et al., 2009b), with an E-W trending axial plane buried beneath approximately 450m of cover that separates them (Figure 4). The northern exposed hill gives strong evidence of steeply south dipping, igneous layering (Figure 4, 8h). The southern exposed hill, however, provided little igneous layering and the structural orientation of the volcanic units are poorly constrained. Detailed mapping has also shown that the volcanic units do not repeat either side of the proposed axial plane. Therefore mapping within the Barnard Rocks area does not support the existence of a syncline fold axis at this locality. The volcanic rocks within this region are strongly broken up along multiple (at least 5) fracture planes with various orientations (Figure 8f). However 2 dominant sets of fracture planes exist with a mostly E-W and N-S orientation (Figure 8g). The relationship between and timing of these fracture sets was difficult to determine.

4. Microstructural analysis and petrology

Ten orientated polished thin sections were made by Pontifex & Associates from deformed volcanic rocks at Mount Jane. Four of these sections were from well foliated and slightly sheared rhyolites, another four from mylonitic rhyolite, one from the zone of ultramylonitic rhyolite and one from a highly foliated and sheared meta-andesite, adjacent the zone of ultramylonite. Sample locations are shown in Figure 2.

4.1. Foliated rhyolite

Four thin sections belong to the foliated rhyolite and include samples 191702, 191703, 191704 and 191707, all of which come from south of the mylonite zone, south Mount Jane (Figure 2). These rhyolites have a porphyritic texture (Figure 9) with equal amounts of plagioclase (simple and multiple twinning) and microcline (cross-hatch twinning) phenocrysts. The phenocrysts are typically 1-4mm in diameter with some as large as 6mm and constitute 10-15% of the rock mass. The matrix supporting the phenocrysts is dominated by crystals of quartz (<0.3mm in size), making up 30-40% of the rock mass. The remainder of the matrix consists of hornblende (up to 35%), with lesser amounts of biotite and plagioclase and trace quantities of opaque minerals and epidote. The biotite is typically a brown/straw brown colour, elongated and in conjunction with the darker green hornblende help define the microscopic foliation (Figure 9a-d). Quartz crystals within the matrix have been elongated in the foliation plane to produce an aspect ratio of 1.5-2:1. Phenocrysts of both microcline and plagioclase have inclusions of quartz, smaller plagioclase and biotite, which lack a preferred orientation (Figure 9a, b), and thus formed prior to, and have been shielded from the deformation. Also to note is the replacement of plagioclase with hornblende and to a lesser degree epidote, particularly on the phenocryst rims.

Both observed in outcrop and thin section are rafts of brown material, approximately 2-8mm in length, which are entrained within the rhyolite. Under thin section the xenoliths appear as dominantly dark brown, mostly hornblende and biotite in composition, but include 1-2mm phenocrysts of plagioclase and smaller crystals of quartz. The rafts are elongated in alignment with the foliation plane. These rafts are interpreted to be sourced from the country rock, with which the volcanic rock flowed through and over and likely had sedimentary or volcanic origins.

Evidence of shearing is preserved, and shear sense only expressed by rotated phenocrysts (δ-clast kinematic); examples from the foliated rhyolite are shown in Figures 9a, b. Shear sense indicators proved difficult to determine in both thin-section and outcrop, but where observed nearly always indicated sinistral sense of movement. When orientated back to outcrop, this indicates a normal (‘north side down’) sense of movement within the shear zone (Figure 3). No microscopic igneous banding was observed within these sections and rare, weakly folded 0.5mm wide quartz veins are present.

4.2. Mylonitic rhyolite

Four thin sections were made from the mylonitic rhyolite, including samples 191705, 191713, 191715 and 191736. Locations of these samples are given in Figure 2. Two of these samples, 191705 and 191715, have mineralogies and textures near equivalent to the before mentioned foliated rhyolite, apart from a slight increase in the proportion of matrix quartz (40-55% of whole rock mass) and the near complete absence of any hornblende (<1%). Also to note is introduction of garnet and the greater concentration of epidote (3-6%), both of which are observed to be replacing phenocrysts of plagioclase (Figure 9e). The strain in these samples is greater than that in the foliated rhyolite with quartz in the matrix slightly more elongated than in the foliated rhyolite. Both the matrix quartz and plagioclase phenocrysts have been slightly reduced in size, compared to the foliated

rhyolite (Figure 9c). Sample 191713 differs fairly dramatically to the other mylonites in that it has very little or no phenocrysts of plagioclase or microcline and instead has been replaced with large clasts of quartz and contains relict micro igneous layering (Figure 9g). Banding between dominantly fine-grained quartz, biotite and muscovite followed by a quartz-rich layer define this igneous layering (Figure 9g). Clasts of quartz 1-3mm long (Figure 9g), have been elongated parallel to the foliation plane (with an aspect ratio of 2-3:1). This relict banding is nearly aligned with the microscopic foliation, indicating a steep northerly dip of igneous banding (Figure 3). The location of this sample is of interest as it lies near the northern margin of what was interpreted as a rhyolite breccia lens, possibly a hyaloclastite. Therefore the clasts observed in this sample are interpreted to be the upper part of this breccia unit, containing clasts of quartz in a highly quartz dominated matrix (approximately 70% of rock mass). Sample 191736 also differs slightly from samples 191705 and 191715 in the fact that its matrix is much coarser grained in general and contains a greater proportion of phenocrysts (Figure 9h). These subtle variations in what is interpreted as the same rock type indicate that the rhyolites at Mount Jane were extruded as a series of separate flows with slight variations in composition.

Strain is variable along and across strike throughout Mount Jane and is sometimes localised to thin 1m wide sections that are strongly deformed whilst only meters away the rock is only slightly deformed (Figure 7a). In thin section, strain appears to be partitioned in much the same way with regions that are shielded from the deformation behind or in front of larger phenocrysts producing non-fibrous pressure shadows (Figure 9f). However, adjacent and between phenocrysts of plagioclase, the strain is focused as the fabric has been forced to flow around and between the more rigid obstacles. Figure 9h shows an example of strain localisation, where the region between the two phenocrysts parallel to the structural fabric has been shielded from the deformation by the more rigid plagioclase crystals whilst immediately above and below this zone the strain is much stronger within the finer quartz-rich matrix and the crystals are elongated and reduced from their original size. It is therefore likely that the greater amount of strain at Mount Jane has been taken up by these samples, causing mylonitisation, instead of the foliated rhyolite due to the greater proportion of fine-grained quartz in the matrix and fewer plagioclase phenocrysts.

All four of the mylonitic rhyolite samples also contain a greater proportion of epidote and muscovite growth, and for sample 191715 (located adjacent the zone of highest strain, Figure 2), garnet (up to 3%). Garnet and epidote is observed replacing phenocrysts of plagioclase (Figure 9e). This fact alone places the deformational event at, at least lower amphibolite facies metamorphism, as a relatively low-P and moderate-T event. The epidote is slightly elongated in the foliation plane, therefore grew synchronously with the deformational event. Garnet however, does not appear to exhibit a preferred orientation and in rare instances is replacing epidote, but is spatially related to the higher strain zones, therefore likely formed during the later stages of deformation. Shear sense within these samples is once again expressed by rotation of phenocrysts and one σ-clast. All rotated phenocrysts give sinistral (north-side down) sense of movement. An example of a δ-clast kinematic indicator from this sample with sinistral sense of shear is displayed in Figure 9d.

4.3. Ultramylonite

This sample (191711) comes from the ESE trending ultramylonite between Mount Jane and Mount Maria (Figure 2). The mineral assemblage is near equal to the rest of the rhyolite samples but varies slightly in proportion. Plagioclase and microcline phenocrysts are less abundant and noticeably smaller (thus reduced in size), measuring 0.3-1.2mm in the ultramylonite, whilst quartz makes up the majority of the rock mass (approximately 40-50%). The remainder of the matrix, in order of abundance comprises biotite, plagioclase, muscovite, garnet and opaque minerals. The extent of mineral elongation in this sample is very strong. Similarly to the mylonitic rhyolite, garnet and epidote minerals are frequently observed replacing the larger phenocrysts of plagioclase in this sample attributed to amphibolite facies metamorphism during deformation. Metamorphic growth of garnet places a minimum temperature of shearing of at least 450ºC, but is likely to have been around 500-550 ºC (D Kelsey pers. comm. 2009). Garnet growth is temporally associated with the mylonitic fabric development and no where else, therefore formed as a result of the deformational event. All asymmetrical kinematic indicators in this sample were rotated porphyroblasts, and show sinistral sense of movement (north side down). An example of such for this sample is given in Figure 9c.

4.4. Meta-andesite

This sample (191709) was collected from a highly deformed region of Mount Jane, adjacent to the ultramylonite zone (Figure 2). The meta-andesite outcrop was strikingly different from the remainder of the rocks at Mount Jane, due to its much more mafic component and originally thought to be a mafic dyke. Analyses of the polished thin section, however, reveal that the composition is dominated by fine-grained, dark coloured hornblende, comprising approximately 40% of the rock mass. There are also large (up to 2mm), blue, radiating porphyroblasts of chlorite. The rest of the matrix consists of up to 30% fine-grained (<0.3mm) quartz and biotite. Other minor mineral occurrences which are observed replacing both hornblende and chlorite is epidote and opaque minerals. The radiating chlorite needles cut across the foliation but have a long crystal axis parallel to the foliation plane and contain inclusions of epidote and quartz, therefore considered to grow syn-deformational. Chlorite, a very water-rich metamorphic mineral is observed replacing hornblende (a more anhydrous mineral), indicating retrograde/retrogressive metamorphism. The presence of chlorite suggests some degree of alteration and therefore, presence of some fluids during or slightly after metamorphism. Given the mineral assemblage, variable thickness and departure of this unit along strike (ie. a lens) indicate that this unit likely resembles an intermediate-mafic composition volcanic flow, probably an andesite.

The sample has moderate to strong elongation of quartz crystals and strong alignment of biotite and hornblende with the microscopic foliation. This elongation and alignment of minerals is in the same orientation as the nearby rhyolite, indicating that it was extruded before the deformational event. Kinematics are poorly developed, due mostly to the absence of phenocrysts, and thus asymmetric features are non-existent in this sample.

5. Secondary Ion Mass Spectrometry (SHRIMP) U-Pb geochronology

5.1. Analytical techniques

Representative samples for geochronology analysis were selected from the outcrop based on their degree of weathering and lack of contamination from other sources. The spatial distributions of the samples are shown in Figure 2. All crushing and mineral separation of the samples was undertaken at the Mawson Laboratories at the University of Adelaide, South Australia. Larger pieces of rock were broken up by a sledge-hammer into fist sized representative portions and were crushed into small fragments using the jaw crusher. The jaw crusher was dissembled and thoroughly cleaned between each sample to avoid cross contamination. The cm-sized fragments were further crushed into fine-grained material using the tungsten-carbide rings in a vibrating mill. The resultant crushing was sieved simultaneously through 75 and 425μm mesh. The 75-425μm fraction was further reduced in size through hand panning using water and detergent to remove dust and separate the denser mineral components. Zircon extraction was accomplished through heavy liquid separation and then passed over with a strong hand magnet to remove highly magnetized material. Approximately 80-120 zircons from each sample were hand picked and, along with several standard grains, were positioned in a 25mm diameter araldite-epoxy mount. The mount was polished to the approximate half-width of the zircon grains.
The polished zircon mounts were then imaged using the Philips XL20 scanning electron microscope (SEM), fitted with a Gatan cathodoluminescence (CL) detector operating at 12.0 kV, located at Adelaide Microscopy, University of Adelaide. A combination of both CL and BSE detectors were used to image the internal zoning and zircon morphology. The mount was then evaporatively coated with about 500 nm of high purity gold for use on the Sensitive High Resolution Ion Microprobe (SHRIMP).
U-Th-Pb zircon analyses of the three samples were collected using the SHRIMP II (B) in the John de Laeter Centre for Mass Spectrometry at Curtin University, Perth, over one session on the 10th September, 2009. The operating guidelines regarding the SHRIMP are detailed in various publications (e.g., Compston et al., 1992; Williams, 1998). Analysis spot locations were chosen based on a combination of CL and optical imagery and aimed for homogenous luminescence regions of the zircon with no inclusions, cracks or imperfections, which could introduce anomalous amounts of ^{206}Pb. A beam diameter of 30μm was used, and prior to analysis, each spot was rastered for 120 seconds to remove any surficial common lead. Five scans were run for each analysis spot and the results were averaged. Common-Pb corrections were applied to all analyses using contemporaneous common-Pb isotopic compositions determined according to the Pb isotopic model of Stacey and Kramers (1975), and these data are presented in Tables 1-3 and Figures 11-13.

5.2. Sample descriptions

Several examples of zircon morphologies, spot analysis locations and age determinations are shown in Figure 10. The degree of luminescence under CL is governed by the concentration of certain trace elements (e.g. U, Hf, Th) within the structure of the zircon.

The zircons in these samples had a range of luminescence and the more intense and brighter zircons generally had less concentration of radioactive trace elements in them.

5.2.1. 191706

This sample was taken from a relatively high strain region within the zone of ultramylonite deformation and preserves high angle structural fabrics. This sample contained mostly pink and glassy zircons ranging from 100-300μm in length with an aspect ratio of 2.5:1, are sub to euhedral in shape and commonly fractured and broken up. CL imagery shows moderately well developed idiomorphic oscillatory zoning in a majority of the crystals and common opaque inclusions. In many cases thin bright, structureless rims surround the zircons (Figure 10a).

5.2.2. 191716

This sample was taken from the undeformed centre of a micro-granite pluton that has intruded into the ultramylonite rhyolite on Mount Jane (Figure 2). This sample proved to be more zircon-rich relative to the other samples. The zircons are smaller (70-150μm) in length, very glassy, clear to slightly pink in colour, stubby (with an aspect ratio of 1.5-2:1) and mostly euhedral in shape. Under CL nearly all the zircons have oscillatory zoning and many contain opaque inclusions (Figure 10b). They appear quite undamaged and transparent.

5.2.3. 191728

Sample 191728 was collected from the same Mount Jane rhyolite, but located about 500m to the south, clear of the shear zone deformation (Figure 2). The zircons in this sample had a similar morphology to sample 191706 with common inclusions, yet slightly smaller in size ranging from approximately 60-250μm in length. The majority of zircons had primary oscillatory zoning structures under CL analysis, but few retain their original crystal shape and are quite broken and fragmented. Examples of some of the zircons and analysis spot locations are shown in Figure 10c.

5.3. Results

All the analytical data of the three samples are presented in Tables 1-3 and diagrammatic representations of the data are displayed in Figures 11-13. All individual spot analyses are shown with an error given to the 1σ level, whilst the error for the grouped data is given at the 2σ level. The age determinations shown in Tables 1-3 and Figures 11-13 have been corrected for ^{204}Pb (common lead), the effect of common lead however is relatively minor. The proportion of common lead (^{204}Pb) in the analyses was minimal with an average of 0.09% of total Pb and ranged from 0 to 0.3% (excluding one anomalously high 0.886% proportion) and did not decrease during the 13 minute analysis, indicating the majority of lead is inherent to the zircon rather than the mount surface.

5.3.1. 191706

15 analyses from 15 separate zircons were conducted on sample 191706 with one analyses located on a highly luminescent metamorphic rim (15.1). The analyses data are displayed in Table 1. The grouped average of the 14 oscillatory zoned targets yielded a weighted mean average ^{204}Pb corrected ^{238}Pb/^{206}U age of 1077±8 Ma (Figure 11a), with a reasonable MSWD of 1.3. However the same 14 analyses yielded a much younger ^{204}Pb corrected ^{207}Pb/^{206}Pb age of 1052±13 Ma and MSWD of 0.7. The ^{204}Pb corrected ^{238}Pb/^{206}U age of the single rim analysis was 1055±17 Ma with a 1σ confidence level, slightly younger than, but within error of, the magmatic cores. The linear regression through the corrected ^{238}U/^{206}Pb vs. ^{207}Pb/^{206}Pb isotope ratios produced an age of 1073±7 Ma for the 14 oscillatory zoned cores when plotted on a Tera-Wasserburg Concordia diagram (Figure 11b), with a slightly higher MSWD of 1.6. Because of the fact that the analyses of the rim in spot 15.1 yielded no significant difference in age, the data all fall into a single population with a corrected ^{238}U/^{206}Pb vs. ^{207}Pb/^{206}Pb isotope ratio age of 1073±7 Ma and MSWD of 1.6, when plotted on a Tera-Wasserburg concordia diagram (Figure 11b), identical to the age excluding analyses 15.1. A number of attempts to date the thin, highly luminescent zircon rims were made, but each time the concentration of common lead (^{204}Pb) was extremely high and the analyses was aborted. This could be attributed to damage of the outer rim and introduction of ^{204}Pb from external sources to the outer rim structure.

5.3.2. 191716

10 analyses of 10 separate zircons were conducted on sample 191716 with the data displayed in Table 2. One analysis (7.1) is excluded from the grouped weighted average of the ^{204}Pb corrected ^{238}Pb/^{206}U age on the basis of that it is significantly discordant from the remainder of the data (Figure 12 a). Thus an age of 1070±6 Ma was determined, with a reasonably good MSWD of 1.1. Similarly, excluding analysis 7.1, the Tera-Wasserburg concordia plot for the corrected ^{238}U/^{206}Pb vs. ^{207}Pb/^{206}Pb isotope ratios produced an age of 1070±5 Ma, with a reasonable MSWD of 1.2 (Figure 12b). These near identical age estimates probably reflect the negligible common Pb detected during the analyses (f 204 = 0.02 avg.), greatly reducing the influence of an inaccurate ^{204}Pb correction. This sample was comparatively high in radioactive isotopes when compared to the other samples with an average ^{238}U and ^{232}Th concentration of 856 and 1109 ppm respectively.

5.3.3. 191728

15 analyses of 15 separate zircons were conducted on sample 191728 with the data displayed in Table 3. Two analyses were excluded (14.1 and 15.1) from the grouped weighted average of the ^{204}Pb corrected ^{238}Pb/^{206}U age on the basis that they were significantly discordant from the remainder of the data (Figure 13a). Expulsion of these two points yielded a ^{238}Pb/^{206}U age of 1069±9 Ma and a low MSWD of 0.61. The Tera-Wasserburg concordia plot for the corrected ^{238}U/^{206}Pb vs. ^{207}Pb/^{206}Pb isotope ratios produced an age of 1071±8 Ma for the 13 concordant analyses, with a reasonable MSWD of 1.3 (Figure 13b). The weighted average corrected ^{207}Pb/^{206}Pb ratio produces an age of

1076±21 Ma (MSWD = 1.9). The disconcordancy of analyses 14.1 and 15.1 along with their significant error (Table 3) can be attributed to the fact that the SHRIMP B software froze up and had to be re-booted and therefore operating conditions were still being optimized during their analyses.

5.4. Interpretation of results

The main constraint on the age of deformation at Mount Jane is the crystallisation age of the cross-cutting and syn-tectonic micro-granite, sample 191716. Zircons from this granite have very well preserved idiomorphic oscillatory zoning which have been interpreted to represent the age of crystallisation of the granite pluton. The strong agreement between both the corrected $^{238}U/^{206}Pb$ vs. $^{207}Pb/^{206}Pb$ and $^{238}Pb/^{206}U$ ages of 1070±5 Ma probably reflects the fact that the zircon structure has been undamaged since its crystallisation and had no introduction of ^{204}Pb. The morphology of the zircons appear quite pristine in comparison to samples 191706 and 191728. The higher concentration of radioactive trace elements (^{238}U and ^{232}Th concentration of 856 and 1109 ppm, average respectively) within the zircons of the granite compared to the encompassing rhyolite, sample 191706 (^{238}U and ^{232}Th concentration of 185 and 194 ppm, average respectively), coupled with the different morphologies of the zircon crystals between the two suggests that there has been little or no inheritance within the granite pluton. The absence of rims corresponding to later zircon growth implies that the zircons show no evidence of high strain contained within the centre of the granite pluton, where the sample was taken.

Sample 191706 also yielded a quite similar, yet slightly older corrected $^{238}U/^{206}Pb$ vs. $^{207}Pb/^{206}Pb$ isotope ratios age of 1073±7 Ma for 14 analyses. This age is interpreted to represent the age of crystallisation of the rhyolite flow that hosts the intruding granite. Under CL, many of the zircons in sample 191706 had thin, highly luminescent structureless rims (Figure 10a). Many of these rims were often more rounded and anhedral surrounding a more euhedral core, suggesting that the rims grew during some phase after crystallisation of the rhyolite, likely during metamorphism. Dating of these rims proved difficult, due to the high concentration of ^{204}Pb (common lead), with only one of five analyses conducted successfully (15.1). This one analyses yielded a slightly younger (but within 1σ error), much less certain (due to $f\,204 = 0.886$) $^{238}Pb/^{206}U$ age of 1055±17 Ma and an even more extreme corrected $^{207}Pb/^{206}Pb$ age of 1008±70 Ma. The high concentration of common lead within the zircon rims is interpreted to be caused by damage to the outer rim and introduction of ^{204}Pb from external sources (e.g. soils). Although there was only one analyses successfully conducted on the thin outer zircon rims, it is interpreted that this rim represents growth from Zr-rich fluids during a phase of deformation and metamorphism during or soon after extrusion of the rhyolite.

Sample 191728, similarly to sample 191706, yielded a corrected $^{238}U/^{206}Pb$ vs. $^{207}Pb/^{206}Pb$ isotope ratio age of 1071±8 Ma for 13 analyses on primary oscillatory zoning within the zircon (Figure 13b). This sample came from the same rhyolite, but 500m south of Mount Jane, out of the zone of shearing (Figure 2). This age is therefore interpreted to likewise, represent the age of crystallisation of the rhyolite flow in the Mount Jane region.

6. Discussion

6.1. Timing of extrusion of the Smoke Hill Volcanics

Prior to this study, age constraints on the deposition of the Smoke Hill Volcanics have been extremely poor. Glikson et al. (1996) obtained a zircon magmatic $^{207}Pb/^{206}Pb$ age of 1078±5 Ma from an outcrop mapped as a rhyolite south of Blackstone Range. Re-assessment of this outcrop by Smithies et al. (2009a) indicated that this rock was actually a fine to medium-grained hornblende and biotite bearing leucogranite, which intrudes as dykes and larger-scale plutons south of Blackstone and Bell Rock Ranges (eg. Tollu Pluton, South Hill Pluton). The leucogranite veins and dykes are temporally and spatially associated with the massive gabbros that locally intrude and engulf the layered intrusions (Smithies et al., 2009a), therefore the 1078±9 Ma age provides a minimum constraint on emplacement of the layered Giles Complex. From recent re-mapping of the west Musgrave Block a victric dacite was sampled approximately 7km due west of Mount Jane and yielded a U-Pb age of 1026±26 Ma (Figure 1b). This age is a sharp contrast to the SHRIMP U-Pb age of 1073±7 Ma attained for the rhyolites at Mount Jane. Therefore this older rhyolite possibly defines a significant time-gap (~50 Ma) in extrusion of the felsic volcanics within the Bentley Supergroup. A series of later-stage faults have dissected the Tollu Group south of Blackstone Range (Smithies et al., 2009b) one of these being a large N-S trending normal fault just west of Mount Jane (Figure 1b) (H Smithies pers. comm. 2009). It is possible that the ~1026 Ma age attained for the vitric dacite represents part of the Smoke Hill Volcanics which has been downthrown relative to Mount Jane and has therefore exposed stratigraphically higher rocks within the volcanic sequence to the west of this fault.

Correlated with the Tollu and Kunmarnara Group volcanic rocks, based on strong similarities in lithological sequence and age is the Tjauwata Group, which straddles the Western Australian and Northern Territory borders, north of the Woodroffe Thrust (Figure 1a) (Edgoose et al., 2004). The 1073±7 Ma age for the Mount Jane rhyolite is similar to the depositional age (and possibly an equivalent) of the Puntitjata Rhyolite within the Tjauwata Group, which yields an age of 1075±3 Ma (Edgoose et al., 2004). It is also interesting to note that the Wankari Volcanics of the Tjauwata Group, a series of porphyritic felsic volcanics interlayered with minor mafic volcanic units (correlated to the Hogarth Formation) (Close et al. 2003) have been ^{207}Pb-^{206}Pb zircon evaporation dated at 1041±2 Ma. This age, therefore also defines a time-gap in deposition of the Tjauwata Group of ~30 Ma from the Puntitjata Rhyolite, which is similar to the time gap in the correlated Tollu Group. Thus it appears as though extrusion of both the Tollu Group and Tjauwata Group occurred as at least two separate episodes of magmatism.

The layered mafic intrusions (including Blackstone Range) have been macroscopically folded to at least some degree prior to, and possibly during the emplacement of the Tollu Group volcanics, evident by tilting of igneous layering of the Giles Complex into the steeply dipping remnants currently exposed. The Blackstone Intrusion, for example, dips 81º to the south on its eastern edge. The age of the Kunmanara Group which the layered

Giles Complex intrudes is very poorly constrained. The youngest detrital age of 1172±8 Ma (weighted $^{207}Pb/^{206}Pb$ age of 36 grains) defines the maximum age for deposition of the MacDougall Formation, which forms the base of the Kunmanara Group. A latest Musgravian Orogeny age of c. 1170 Ma defines a similar maximum age constraint to the c. 1172 Ma detrital age for the deposition of the Kunmanara Group (and Giles Complex). If the Tjauwata Group is indeed a correlative of the Bentley Supergroup then the 1084±9 Ma Walu Granite (Close et al., 2003) which intrudes the Mount Harris Basalt (correlative of the Mummawarrawarra Basalt) therefore provides a minimum age constraint for the deposition of the Kunmanara Group. The Giles Complex however is very poorly constrained and could have intruded the Kunmanara Group of the Western Musgrave Block any time between ~1170 and 1075 Ma. The Giles Complex and Kunmanara Group on BLACKSTONE (Smithies et al., 2009b), evidently was at least broadly folded, uplifted and eroded, prior to the unconformable extrusion of the rhyolite at Mount Jane at ~1073 Ma. The widespread intrusion of the Giles Complex would have caused large amounts of upper crustal melting, thus producing the multiple felsic magmatic pulses that intrude the mafic-ultramafic layered intrusions and eruptions of the Bentley Supergroup.

6.2. Timing and style of deformation

The best constraint on the age of the deformation at Mount Jane is the syn-tectonic microgranite intrusion (Figure 2). The microgranite which is more crystalline and harder than the rhyolite acted as an obstacle to shearing and has well foliated outer margins where it is in contact with the encompassing finer-grained (and more easily deformed) rhyolite. In close proximity to the intrusion are granite veins that are correlated to the larger body which cross-cut the mylonitic fabric. Therefore these field observations indicate that the microgranite intrusion occured synchronous with the deformational event. SHRIMP U-Pb dating of this granite intrusion yielded an age of 1070±5 Ma. The morphologies of zircons from the granite compared to the rhyolite under CL analysis indicated distinct differences, with much stronger oscillatory zoning, smaller size and the more euhedral shape from the granite sample compared to the rhyolite (Figure 10a-c). The microgranite zircons were also anomalously high in uranium and thorium compared to the rhyolite (Tables 1-3) and therefore the possibility of inheritance of zircons within the granite intrusion is discounted. Chlorite and epidote alteration of hornblende within the meta-andesite adjacent to the ultramylonite, indicate the presence of at least some fluids during the metamorphic event. Therefore it is likely that the thin, luminescent, structureless rims (Figure 10a) that surround the zircons in the highly deformed rhyolite (sample 191706), formed during metamorphism from zirconium-bearing fluids. Dating of one of these outer rims gave a $^{206}Pb/^{238}U$ age of 1055±17 Ma, with a 1σ error (Table 1, 706-15.1). The steeply south dipping mylonitic fabric therefore formed during or soon after the time of extrusion (~1072 Ma), and probably continued for some time after. However the age of both the microgranite intrusion and extrusion of the rhyolite at Mount Jane is within error of each other and separation of the two events is outside the scope of the SHRIMP U-Pb analysis system. Therefore this study agrees with the hypothesis of many workers (e.g. Clarke et al., 1995; Stewart, 1995; Glikson et al., 1996; Smithies et al., 2009a) that the Giles Event was accompanied by a period of strong deformation, which continued to at least the early stages of extrusion of the Tollu Group volcanics. However

this study has successfully dated field relationships that constrain this Giles Event period of deformation.

The location of the highest strain is interestingly located where, in thin-section, the highest proportion of quartz in the matrix occurs. This may have caused the loci of strongest deformation at Mount Jane due to the preferential ease at which quartz is deformed. The microgranite intrusion into the shear zone (Figure 2) may also have also aided deformation and development of the observed mylonitic foliation by the addition of heat causing the at least lower amphibolite facies metamorphism indicated in thin-section. In thin-section, epidote appeared slightly elongated in some sections and garnet sub-euhedral and undeformed, thus indicating that peak metamorphic conditions were achieved at a short time after the phase of deformation. This peak metamorphic grade was followed by retrograde/retrogressive metamorphism indicated by replacement of amphibole by more hydrous metamorphic chlorite in the meta-andesite. Throughout the Mount Jane shear system distinct structural fabrics and linear elements vary and seem to correlate and respond to the different strain gradients. Highly strained mylonitic zones preserve well developed rotational strain (i.e. delta clasts) (Figure 9) and mineral stretching lineations which are perpendicular to the inferred bulk shearing direction (Figure 2) in the lower strained zones and high angle structural fabrics. In contrast, the lower strained zones exhibit more shallow-dipping structural fabrics (Figure 2) and poorly developed rotational strain indicators and linear fabrics (mineral stretching lineation) which parallels the bulk shearing direction (north-side down). Such variability in structural and linear elements is usually attributed to simultaneous simple and pure shearing resulting in partitioning of strain into coaxial and non-coaxial components (Fossen and Tikoff, 1993). The progressive change in orientation of the stretching lineation between high and low strain zones (interpreted to be equivalent to high and low rotational strain) (Figure 2) is interpreted to represent incremental changes in orientation of the principle axis of the finite strain ellipsoid Therefore the higher strain zones were dominated by simple shear, and developed stretching lineations perpendicular to the bulk tectonic transport direction and alternatively, lower strain zones were dominated by pure shear and developed flattening fabrics and stretching lineations parallel to the shortening direction. The shear sense throughout Mount Jane in both thin-section and outcrop gave ‘north-side down sense of movement. The combination of north-dipping mylonite development in the south of Mount Jane, vertical-dipping ultramylonite in the core, with at least some component of strike-slip movement, and south-dipping mylonite in the north of Mount Jane (Figure 3), gives the appearance of a ‘positive flower-structure’ shear system.

The areal extent and timing of D3 deformation (Giles Event) is poorly known, but is best observed within the western Musgrave Block at close proximities to the layered mafic – ultramafic intrusions (Wade et al., 2008). D3 deformation, where observed is typically manifested by steeply dipping mylonite zones, which re-oriented D2 deformation fabrics, and are cross-cut by ca. 820 Ma Amata Dolerite dykes (Clarke et al., 1992) and in parts appears coeval with emplacement of the ca. 1080 Ma layered mafic-ultramafic intrusions (Glikson et al., 1996). The steeply SW dipping ultramylonite at Mount Jane presented in this study appears closely analogous to a number of the features described for D3 aged

deformation observed elsewhere, such as the Hinckley Fault. Strong structural and geochronological evidence therefore places the age of mylonitic deformation at Mount Jane as late Mesoproterozoic D3 (Giles Event). Overprinting of any younger structural fabrics (e.g. Petermann aged) is not observed within the Mount Jane shear zone.

The southwards dipping Blackstone Range is believed to form the northern limb of an upright, W-plunging structural syncline, with relicts of the southern limb sporadically exposed approximately 20km to the south, immediately north and east of the Cavanagh Range (Figure 1b) (Smithies et al., 2009a, b; Evins et al., in press). If this is indeed true, then both the widespread N-S dipping foliation and W-plunging macroscopic folding (Figure 8b-d) at Mount Jane is consistent with the orientation of the folding within the large-scale mafic-ultramafic layered intrusion, indicating the NNW-trending deformation which folded the layered intrusion, likely continued during the extrusion of the Smoke Hill Volcanics. If the Blackstone Syncline truly exists, then mapping of the core of the syncline, at Barnard Rocks (Figure 4, 5), where the proposed E-W trending axial plane lies, provided inconclusive evidence of its existence. The northern exposed hill at Barnard Rocks, gave strong evidence of steeply south dipping, igneous layering (Figure 4, 8h). The southern exposed hill, however, provided little igneous layering and the structural orientation of the volcanic units are poorly constrained. However, of the many fracture planes observed at Barnard Rocks, a dominant E-W trending fracture set was observed (Figure 8g). This fact, along with the consistently steep, south-dipping igneous layering within the volcanic rocks, suggests that these rocks have also been deformed in a dominantly N-S directed orientation. Due to the un-repeated stratigraphy over the proposed location of the axial plane and the steep southern-dip of the volcanic rocks at Barnard Rocks, it is concluded that the fold axis of the Blackstone Syncline, if it exists must lie slightly to the south of this mapping area. Approximately 5km to the south, igneous layering within the Smoke Hill Volcanics dips moderately towards the north (Figure 1b) (Smithies et al., 2009b). Therefore the possibility exists that either the Tollu Group has been folded about the same axis as the Blackstone Range intrusive as part of the ongoing deformation during the Giles Event or alternatively the Tollu Group volcanics may have flowed down into a topographic basin caused by a pre-existing, at least broadly folded Blackstone Syncline (Evins et al., in press). Detailed mapping within the Blackstone Basin would be required to resolve the origin of the tilted igneous layering in the Tollu Group.

7. Conclusion

The bimodal volcanic rocks of the Giles Event were deposited unconformably on the previously folded layered mafic-ultramafic Blackstone intrusion of the Giles Complex. SHRIMP U-Pb dating of zircon cores of two samples from the Smoke Hill Volcanics rhyolite at Mount Jane yielded ages of 1071±8 Ma and 1073±7 Ma. The 1075±3 Ma Puntitjata Rhyolite of the Tjauwata Group, further to the north, is considered a correlative of the Mount Jane rhyolite based on strong similarities in lithological sequence and age. This age constraint implies that the emplacement of the Giles Complex on BLACKSTONE occurred before unconformable extrusion of the ~1072 Ma rhyolite onto

the layered intrusion at Mount Jane. Prior to the extrusion of these rhyolites observed at Mount Jane the Blackstone Range intrusion was uplifted, eroded and folded.
Very soon after their deposition, or possibly synchronous with their crystallisation, the rhyolites were strongly deformed with the development of a 2km wide NW trending shear zone. These rhyolites were deformed at higher temperatures than their extrusion, indicated by the syn-kinematic garnet and amphibole growth in the mylonites. The minimum temperature for this shearing is 450ºC for garnet growth, but is more likely to be around 500-550ºC. Up to ultramylonite levels of strain were experienced in the near vertical/steeply south-dipping core of the, at least, lower amphibolite facies shear zone. Shear sense indicators, being mostly rotated phenocrysts in both outcrop and thin section consistently indicate north side down sense of shearing. Many features of this shear zone are consistent with D3 aged deformation, observed elsewhere in the western Musgrave Block (eg. Hinckley Fault). A syn-tectonic microgranite intrudes the centre of the shear zone at Mount Jane, with associated granitic veins which cross-cut the mylonitic fabric. Dating of this intrusion yielded an age of 1070±5 Ma. This age, along with the consistent style of deformation with D3, places the shear zone at Mount Jane as Giles Event aged and more importantly, indicates that deformation of the layered mafic-ultramafic intrusions continued well after their emplacement and deformed the overlying Tollu Group. This continued deformation during the emplacement of the Tollu Group may also be responsible for the N-S directed folding of the Hogarth Group, which directly overlies the Smoke Hill Volcanics, or alternatively the steeply dipping igneous layering could have formed as a result of slumping of the volcanics down a topographic basin caused by a pre-existing at least broadly folded, Blackstone Syncline.

8. Acknowledgements

Most of all I would like to thank my supervisors Alan Collins and Martin Hand for all their guidance and help throughout the year. Many thanks go to the GSWA, in particular Hugh Smithies, Heather Howard, Mario Werner and Mario Holmes for their generous logistical, intellectual and financial support and in conjunction with the Ngaanyatjarra Council allowing us access and showing us around the beautiful lands of the western Musgrave Ranges. Also Chris Kirkland and Mike Wingate are thanked for their setting up, running and assistance with the SHRIMP and interpretation of geochronology. I am also indebted to Ben Wade and Angus Netting of Adelaide Microscopy for all their technical expertise. Many thanks also go to Dave Kelsey, Ailsa Woodhouse and Caroline Forbes for taking the time to read my draft, providing valuable feedback and answering my many questions throughout the year. The Australian Institute of Geoscientists is gratefully acknowledged for providing a generous Honours bursary. Finally to the great Honours crew, who made 2009 a memorable and enjoyable year, in particular Alexander Sen for his interesting choice of music, excellent cooking, camaraderie and having to put up with me for a month in the Musgrave Ranges.

9. References

Camacho, A., 1997. An isotopic study of deep-crustal orogenic processes, Musgrave Block, central Australia. *Ph.D. dissertation, Australian National University, Canberra, Australia.*

Camacho, A., Compston, W., McCulloch, M. and McDougall, I., 1997. Timing and exhumation of eclogite facies shear zones, Musgrave Block, Central Australia. *Journal of Metamorphic Geology* 15, 735-751.

Camacho, A. and Fanning, C. M. 1995. Some isotopic constraints on the evolution of the granulite and upper amphibolite facies terranes in the eastern Musgrave Block, central Australia. *Precambrian Research* 71, 155-181.

Camacho, A. and McDougall, I. 2000. Intracratonic, strike-slip partitioned transpression and the formation and exhumation of eclogite facies rocks: an example from the Musgrave Block, central Australia. *Tectonics* 19, 978–996.

Cawood, P.A., 2005. Terra Australis Orogen: Rodinia breakup and development of the Pacific and Iapetus margins of Gondwana during the Neoproterozoic and Paleozoic. *Earth-Science Reviews* 69, 249-279.

Cawood, P.A. and Korsch, R.J., 2008. Assembling Australia: Proterozoic building of a continent. *Precambrian Research* 166, 1-38.

Clark, D.J., Hensen, B.J., Kinny, P.D., 2000. Geochronological constraints for a two stage history of the Albany-Fraser Orogen Western Australia. *Precambrian Research* 102(3–4), 155–183.

Clarke, G.L., 1992. Contact relationships and structure of the Hinckley Gabbro and environs, Giles Complex. Western Musgrave Block, W.A. *AGSO Research Newsletter* 17, 6–8.

Clarke, G.L., Buick, I.S., Glikson, A.Y. and Stewart, A.J., 1995. Structural and pressure temperature evolution of the host rocks of the Giles Complex, western Musgrave Block, central Australia: evidence for multiple high-pressure events. *AGSO Journal of Australian Geology and Geophysics* 16, 127-146.

Close D.F., Edgoose C.J. and Scrimgeour I.R., 2003. Hull and Bloods Range Special, Northern Territory (First Edition). 1:100 000 geological map series explanatory notes, 4748, 4848. Northern Territory Geological Survey, Darwin.

Collerson, K.D., 1972. High grade metamorphic and structural relationships near Amata, Musgrave Ranges, central Australia. Ph.D. Thesis, University of Adelaide, Adelaide.

Collins, A.S. and Pisarevsky, S.A., 2005. Amalgamating eastern Gondwana: The evolution of the Circum-Indian Orogens. *Earth-Science Reviews* 71, 229-270.

Compston, W., Williams, I.S., Kirschvink, J.L., Zichao, Z. and Guogan, M.A., 1992. Zircon U-Pb ages for the Early Cambrian time-scale. *Journal of the Geological Society of London* 149, 171-184.

Daniels, J.L., 1974. The geology of the Blackstone Region of Western Australia. Geological Survey ofWestern Australia, Bulletin, 123.

Edgoose, C.J., Scrimgeour, I. and Close, D., 2004. Geology of the Musgrave Block, Northern Territory. Northern Territory Geological Survey Report, 15.

Evins, P.M., Smithies, H., Howard, H.M., Kirkland, C.L., Wingate, M.T.D. and Bodorkos, S. In press. Devil in the detail; the structural evolution and chronology of a Mesoproterozoic mafic-felsic intrusive province. *Precambrian Research*, in-press.

Fitzsimons, I.C.W., 2003. Proterozoic basement provinces of southern and southwestern Australia, and their correlation with Antarctica. In: Yoshida, M., Windley, B.F., Dasgupta, S. (Eds.), Proterozoic East Gondwana: Supercontinent Assembly and Breakup. *Geological Society of London, Special Publication* 206, 93–129.

Flöttmann, T., Hand, M., Close, D., Edgoose, C. J. and Scrimgeour, I. R. 2004. Thrust tectonic styles of the intracratonic Alice Springs and Petermann Orogenies, Central Australia. In: *Thrust tectonics and hydrocarbon systems* (edited by McClay, K. R.) AAPG Memoir 82, 538-557.

Fossen, H. and Tikoff, B. 1993. The deformation matrix for simultaneous simple shearing, pure shearing and volume change, and its application to transpression-transtension tectonics. *Journal of Structural Geology* 15(3-5), 413-422.

Glikson, A.Y., Stewart, A.T., Ballhaus, G.L., Clarke, G.L., Feeken, E.H.T., Level, J.H., Sheraton, J.W., and Sun, S-S., 1996, Geology of the western Musgrave Block, central Australia, with reference to the mafic–ultramafic Giles Complex: Canberra, *Australian Geological Survey Organisation*, Bulletin 239, 206p.

Goode, A.D.T., 1970. The petrology and structure of the Kalka and Ewarara layered basic intrusions, Giles Complex, central Australia. Ph.D. Thesis, University of Adelaide, Adelaide.

Gray, C.M., 1977. The geochemistry of central Australian granulites in relation to the chemical and isotopic effects of granulite facies metamorphism. *Contributions to Mineralogy and Petrology* 65, 79-89.

Gray, C.M., 1978. Geochronology of granulite-facies gneisses in the western Musgrave Block, Central Australia. *Journal of the Geological Society of Australia* 25, 403-414.

Hand, M. and Sandiford, M., 1999. Intraplate deformation in central Australia, the link between subsidence and fault reactivation. *Tectonophysics* 305, 121-140.

Howard, H.M., Smithies, R.H., Pirajno, F. and Skwarnecki, M.S., 2007. Bell Rock, W.A. Sheet 4645: Geological Survey of Western Australia, 1:100000 Geological Series.

Kirkland, C.L., Wingate, M.T.D., and Bodorkos, S., 2008a. 185509: Geochronological dataset 725, in Compilation of geochronological data: Geological Survey of Western Australia.

Kirkland, C.L., Wingate, M.T.D. and Bodorkos, S., 2008b. 174761: Geochronological dataset 721, in Compilation of geochronological data: Geological Survey of Western Australia.

Major, R.B., Conor, C.H.H., 1993. The Musgrave Block. In: Parker, A.J. (Ed.), The Geology of South Australia, vol. 1. *The Precambrian. Geological Survey South Australia Bulletin*, pp. 156–167.

Morris P.A, and Pirajno F., 2005, Geology, geochemistry, and mineralization potential of Mesoproterozoic sill complexes of the Bangemall Supergroup, Western Australia: Geological Survey of Western Australia, Report 99, 78p.

Moore, A., 1970. The Geology of the Gosse Pile Ultramafic intrusion and of the surrounding granulites, Tomkinson Ranges, central Australia. Ph.D. Thesis, University of Adelaide, Adelaide.

Myers, J.S., Shaw, R.D., Tyler, I.M., 1996. Tectonic evolution of Proterozoic Australia. *Tectonics* 15(6), 1431–1446.

Nesbitt, R.W., Goode, A.D.T., Moore, A.C., Hopwood, T.P., 1970. The Giles Complex, central Australia; a stratified sequence of mafic and ultramafic intrusions, Bushveld igneous complex and other layered intrusions, Symposium. Special Publication, Geological Society of South Africa, pp. 547–564.

Nesbitt, R.W., Kleeman, A.W., 1964. Layered intrusions of the Giles Complex, central Australia. *Nature* (London) 203, 391–393.

Raimondo, T., Collins A.S., Hand, M., Walker-Hallam, A., Smithies, R.H., Evins, P.M. and Howard, H.M., 2009. Ediacaran intracontinental channel flow. *Geology* 37(4), 291–294.

Sandiford, M., 2002. Low thermal Peclet number intraplate orogeny in central Australia. *Earth and Planetary Science Letters* 201, 309-320.

Sandiford, M. and Hand, M. 1998. Controls on the locus of intraplate deformation in central Australia. *Earth and Planetary Science Letters* 162(1-4), 97-110.

Sandiford, M., Hand, M. & McLaren, S. 2001. Tectonic feedback, intraplate orogeny and the geochemical structure of the crust: a central Australian perspective. In: *Continental reactivation and reworking.* (edited by Miller, J. A., Holdsworth, R. E., Buick, I. S. & Hand, M.). *Geological Society of London, Special Publications* 184, 219-236.

Scrimgeour, I. and Close, D., 1999. Regional high-pressure metamorphism during intracratonic deformation: the Petermann Orogeny, central Australia. *Journal of Metamorphic Geology* 17, 557–572.

Smithies, R.H., Howard, H.M., Evins, P.M., Kirkland, C.L., Bodorkos, S., and Wingate, M.T.D., 2009a. The west Musgrave Complex — new geological insights from recent mapping, geochronology, and geochemical studies: Geological Survey of Western Australia, Record 2008/19, 20p.

Smithies, R.H., Howard, H.M., Evins, P.M., and Maier, W.D, 2009b. Blackstone, WA Sheet 4545: Geological Survey of Western Australia, 1:100 000 Geological Series.

Sprigg, R.C., Wilson, R.B., 1959. The Musgrave mountain belt in South Australia. Geological Rundschau 47, 531–542.

Stacey, J.S. and Kramers, J.D. 1975. Approximation of terrestrial lead isotope evolution by a two-stage model: *Earth and Planetary Science Letters* 26, 207–221.

Stewart, A.J., 1995. Resolution of conflicting structures and deformation history of the Mount Aloysius granulite massif, western Musgrave Block, central Australia. AGSO *Journal of Australian Geology and Geophysics* 16, 91–105.

Sun, S. S. and Sheraton, J. W. 1992. Zircon U/Pb chronology, tectonothermal and crust-forming events in the Tomkinson Ranges, Musgrave Block, central Australia. *AGSO Research Newsletter* 17, 9-10.

Sun, S.S., Sheraton, J.W., Glikson, A.Y., and Stewart, A.J., 1996, A major magmatic event during 1050–1080 Ma in central Australia, and an emplacement age for the Giles Complex: *AGSO Research Newsletter* 24, 13–15.

Thompson, B.P., 1975. Musgrave block—regional geology. In: Knight, C.L. (Ed.), Economic Geology of Australia and Papua New Guinea. 1: Metals. The Australian Institute of Mining and Metallurgy pp. 451–454.

Wade, B.P., Barovich, K.M., Hand, M., Scrimgeour, I.R. and Close, D.F., 2006. Evidence for Early Mesoproterozoic Arc Magmatism in the Musgrave Block, Central Australia:

Implications for Proterozoic Crustal Growth and Tectonic Reconstructions of Australia. *Journal of Geology* 114, 43-63.

Wade, B.P., Hand, H. and Barovich, K.M., 2005. Nd isotopic and geochemical constraints on provenance of sedimentary rocks in the eastern Officer Basin, Australia: Implications for the duration of the intracratonic Petermann Orogeny. *Journal of the Geological Society of London* 162, 513-530.

Wade, B.P., Kelsey, D.E., Hand, M.K. and Barovich, K.M., 2008. The Musgrave Province: Stitching north, west and south Australia. *Precambrian Research* 166, 370-386.

White, R.W., Clarke, G.L., Nelson, D.R., 1999. SHRIMP U–Pb zircon dating of Grenvilleage events in the western part of the Musgrave Block, central Australia. *Journal of Metamorphic Geology* 17(5), 465–481.

Williams, I.S., 1998. U-Th-Pb geochronology by ion microprobe. In: M.A. McKibben, W.C. Shanks and W.I. Ridley (Editors), Applications of microanalytical techniques to understanding mineralizing processes. *Reviews in Economic Geology* pp. 1-35.

Wingate, M.T.D., Parajino, F. and Morris, P.A., 2004. Warakurna large igneous province: A new Mesoproterozoic large igneous province in west-central Australia. *Geological Society of America* 32, 105-108.

10. Figure captions

Figure 1 - (a) Regional geological map of the Musgrave Block, showing its position within Australia relative to the state boundaries and Amadeus and Officer Basins. Also shown are the broad domains within the Musgrave Block and locations of the Woodroffe Thrust, Hinckley and Mann Fault. Map modified after Cawood and Korsch (2008); (b) Location of the Mount Jane and Barnard Rocks mapping areas within the BLACKSTONE 1:100 000 series map sheet. Map modified after Smithies et al. (2009b).

Figure 2 - Detailed 1:10 000 geological map of the Mount Jane mapping area showing structural data, sample locations and the NW-trending mylonite and ultramylonite zones.

Figure 3 - Structural N-S orientated cross-section constructed through the Mount Jane shear zone, (location of x-section is displayed on Figure 2).

Figure 4 - Detailed 1:10 000 geological map of the Barnard Rocks mapping area showing structural data and inferred trend of the lithological contacts.

Figure 5 - Structural N-S orientated cross-section constructed through the Barnard Rocks volcanic sequence, (location of x-section is displayed on Figure 4).

Figure 6 – Outcrop photos of lithology taken from various locations within Mount Jane and Barnard Rocks. (a) Small-scale folding of igneous layering indicating volcanic flow; (b) Looking SE at the interpreted unconformable contact of the layered mafic-ultramafic intrusion and Smoke Hill Volcanics rhyolite. To note is the steep east dipping foliation of the mafic rocks, oblique to the more north-dipping rhyolite. Mount Jane is in the background; (c) Looking South at tilted igneous layering within the amygdaloidal basalt approximately 1km south of Mount Jane; (d) Relatively undeformed jigsaw-fit breccia rhyolite, located adjacent ultramylonite. Also observable are round spherulites at the top of the rock; (e) Auto-brecciation of the rhyolite, indicated at Barnard Rocks; (f) Looking north at finely graded (upwards (south) younging) layering in the basalt-breccia unit at Barnard Rocks.

Figure 7 - Outcrop photos of structure taken from various locations within Mount Jane. (a) Strain partitioning within the deformed rhyolite, with poor development of foliation on the rhyolite boulder and strong foliation development and shearing juxtaposed against it; (b) Looking south at a steeply north dipping foliation plane located only 10m north of microgranite intrusion. The granite vein can be seen cross-cutting the foliated rhyolite; (c) Deformed and slightly rotated phenocrysts of plagioclase in mylonitic rhyolite; (d) Looking west at typical outcrop of steeply dipping, strongly developed foliation planes within mylonitic rhyolite; (e) Very well developed stretching lineation in ultramylonite.

Figure 8 – Stereonets and associated contour plot of all the structural data attained from both the Mount Jane and Barnard Rocks mapping areas.

Figure 9 - Photomicrographs of key kinematic indicators and petrological relationships. Figures 9 (a-d) are of rotated phenocrysts of plagioclase and all indicate sinistral sense of shear. All four of these photomicrographs were taken in plane polarised light at 5x zoom except (c) which was taken at 1.5x zoom. Scale bars and location of photo relative to the thin-section and its orientation are provided on the interpreted drawings (right); (e) Replacement of plagioclase phenocrysts by epidote and garnet growth during metamorphism/deformation. Photomicrograph taken in cross-polar light at 10x zoom; (f) Strain shadow directly in front and behind plagioclase phenocrysts as the quartz-rich fabric is forced around the obstacle. Photomicrograph taken in cross-polar light at 1.5x zoom; (g) Igneous depositional micro-layering and elongation of quartz clasts in sample 191713. Photomicrograph taken in plane-polarised light at 1.5x zoom; (g) Micro strain partitioning within mylonitic rhyolite. The quartz crystals between the plagioclase phenocrysts are relatively undeformed whilst immediately above and below them, the fabric is strongly deformed and quartz crystals are elongated in foliation plane and reduced in size. Photomicrograph taken in cross-polar light at 1.5x zoom.

Figure 10 - Cathodoluminescence images of representative zircon grains extracted from (a) sample 191706; (b) sample 191716; (c) sample 191728. Displayed spot ages are $^{206}Pb/^{238}U$ ages, and spot size shown is 30μm.

Figures 11-13 - Diagrammatic representations of SHRIMP zircon age data from 11(a, b) sample 191706; 12(a, b) sample 191716; 13(a, b) sample 191728. $^{238}Pb/^{206}U$ weighted average using ^{204}Pb-corrected age estimates are displayed on the left (a) and right (b), the Tera-Wasserburg concordia plot using uncorrected isotope ratios of $^{238}Pb/^{206}U$ Vs. $^{207}Pb/^{206}Pb$ with anchor value for the linear regression is also shown with its associated error.

11. Tables

Grain Spot no.	^{238}U (ppm)	^{232}Th (ppm)	$^{232}Th/^{238}U$	f^{204} (%)	$^{238}U/^{206}Pb^*$ ±1σ		$^{207}Pb^*/^{206}Pb^*$ ±1σ		$^{238}U/^{206}Pb^*$ date (Ma)	±1σ	$^{207}Pb^*/^{206}Pb^*$ date (Ma)	±1σ	Disc (%)
706-1.1	171	184	1.11	0.116	5.490	0.062	0.07433	0.00103	1079	13	1050	28	-2.7
706-2.1	188	206	1.13	-0.105	5.387	0.059	0.07480	0.00096	1098	13	1063	26	-3.2
706-3.1	215	166	0.80	0.246	5.647	0.059	0.07392	0.00107	1051	12	1039	29	-1.1
706-4.1	245	286	1.21	0.107	5.415	0.054	0.07360	0.00085	1092	12	1030	23	-6.0
706-5.1	222	275	1.28	0.116	5.456	0.055	0.07506	0.00089	1085	12	1070	24	-1.4
706-6.1	244	295	1.25	0.000	5.431	0.054	0.07485	0.00073	1089	12	1065	20	-2.3
706-7.1	192	174	0.94	0.140	5.448	0.059	0.07362	0.00101	1086	13	1031	28	-5.4
706-8.1	129	129	1.03	0.156	5.561	0.070	0.07442	0.00125	1066	15	1053	34	-1.2
706-9.1	133	151	1.18	-0.048	5.468	0.067	0.07574	0.00105	1083	15	1088	28	0.5
706-10.1	233	245	1.08	0.176	5.573	0.056	0.07391	0.00097	1064	12	1039	26	-2.4
706-11.1	215	234	1.12	0.032	5.575	0.057	0.07366	0.00082	1064	12	1032	22	-3.0
706-12.1	171	169	1.02	0.077	5.593	0.063	0.07414	0.00098	1060	13	1045	27	-1.4
706-13.1	148	167	1.16	0.042	5.545	0.065	0.07577	0.00097	1069	14	1089	26	1.8
706-14.1	176	186	1.09	0.143	5.440	0.060	0.07348	0.00102	1088	13	1027	28	-5.9
706-15.1	93	44	0.49	0.886	5.624	0.081	0.07277	0.00250	1055	17	1008	70	-4.7

Table 1– SHRIMP zircon age data for sample 191706

Grain Spot no.	^{238}U (ppm)	^{232}Th (ppm)	$^{232}Th/^{238}U$	f^{204} (%)	$^{238}U/^{206}Pb^*$ ±1σ		$^{207}Pb^*/^{206}Pb^*$ ±1σ		$^{238}U/^{206}Pb^*$ date (Ma)	±1σ	$^{207}Pb^*/^{206}Pb^*$ date (Ma)	±1σ	Disc (%)
716-1.1	878	780	0.92	0.013	5.550	0.039	0.07525	0.00035	1068	8	1075	9	0.7
716-2.1	512	602	1.21	0.025	5.514	0.046	0.07555	0.00051	1074	10	1083	14	0.8
716-3.1	520	686	1.36	-0.013	5.651	0.047	0.07576	0.00051	1050	9	1089	13	3.5
716-4.1	504	643	1.32	0.000	5.494	0.046	0.07557	0.00050	1078	10	1084	13	0.5
716-5.1	1177	1228	1.08	0.022	5.494	0.039	0.07484	0.00034	1078	8	1064	9	-1.3
716-6.1	2063	3253	1.63	0.015	5.513	0.037	0.07475	0.00028	1075	8	1062	8	-1.2
716-7.1	1343	1933	1.49	0.013	5.360	0.037	0.07466	0.00030	1103	8	1059	8	-4.1
716-8.1	508	721	1.46	0.000	5.576	0.046	0.07474	0.00047	1063	9	1061	13	-0.2
716-9.1	460	579	1.30	0.054	5.499	0.046	0.07412	0.00056	1077	10	1045	15	-3.1
716-10.1	589	668	1.17	0.072	5.595	0.045	0.07507	0.00051	1060	9	1070	14	1.0

Table 2 – SHRIMP zircon age data for sample 191716

Grain Spot no.	^{238}U (ppm)	^{232}Th (ppm)	$^{232}Th/^{238}U$	f^{204} (%)	$^{238}U/^{206}Pb^*$ ±1σ		$^{207}Pb^*/^{206}Pb^*$ ±1σ		$^{238}U/^{206}Pb^*$ date (Ma)	±1σ	$^{207}Pb^*/^{206}Pb^*$ date (Ma)	±1σ	Disc (%)
728-1.1	242	293	1.25	0.135	5.489	0.070	0.07440	0.00088	1079	15	1052	24	-2.5
728-2.1	134	151	1.17	0.142	5.555	0.082	0.07532	0.00119	1067	17	1077	32	0.9
728-3.1	124	145	1.21	0.246	5.574	0.084	0.07403	0.00135	1064	17	1042	37	-2.1
728-4.1	175	193	1.14	0.108	5.510	0.076	0.07530	0.00099	1075	16	1076	26	0.1
728-5.1	128	124	1.00	0.245	5.547	0.082	0.07333	0.00134	1069	17	1023	37	-4.4
728-6.1	135	150	1.15	0.298	5.491	0.081	0.07259	0.00142	1079	17	1003	40	-7.6
728-7.1	264	304	1.19	0.049	5.647	0.071	0.07546	0.00075	1051	14	1081	20	2.8
728-8.1	109	128	1.21	0.113	5.517	0.086	0.07435	0.00124	1074	18	1051	34	-2.2
728-9.1	234	285	1.26	0.027	5.665	0.073	0.07754	0.00077	1048	15	1135	20	7.7
728-10.1	256	366	1.48	0.054	5.523	0.070	0.07656	0.00081	1073	15	1110	21	3.4
728-11.1	180	211	1.21	0.000	5.414	0.280	0.07447	0.00082	1093	61	1054	22	-3.6
728-12.1	168	202	1.24	0.000	5.534	0.075	0.07570	0.00085	1071	16	1087	22	1.5
728-13.1	141	107	0.78	0.000	5.369	0.095	0.07396	0.00094	1101	21	1040	26	-5.8
728-14.1	166	184	1.14	0.000	5.663	0.355	0.07191	0.01934	1048	71	983	547	-6.6
728-15.1	144	165	1.18	0.000	6.624	5.872	0.07570	0.00087	906	810	1087	23	16.6

Table 3 – SHRIMP zircon age data for sample 191728

12. Figures

Figure 1(a)

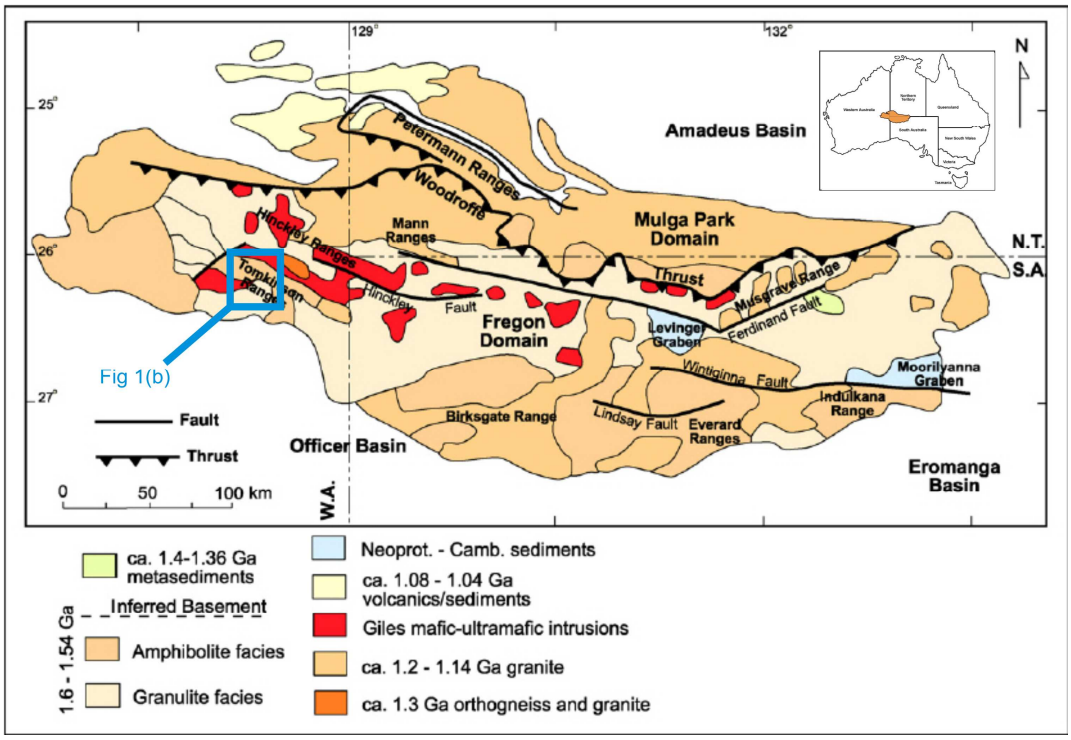

(b)

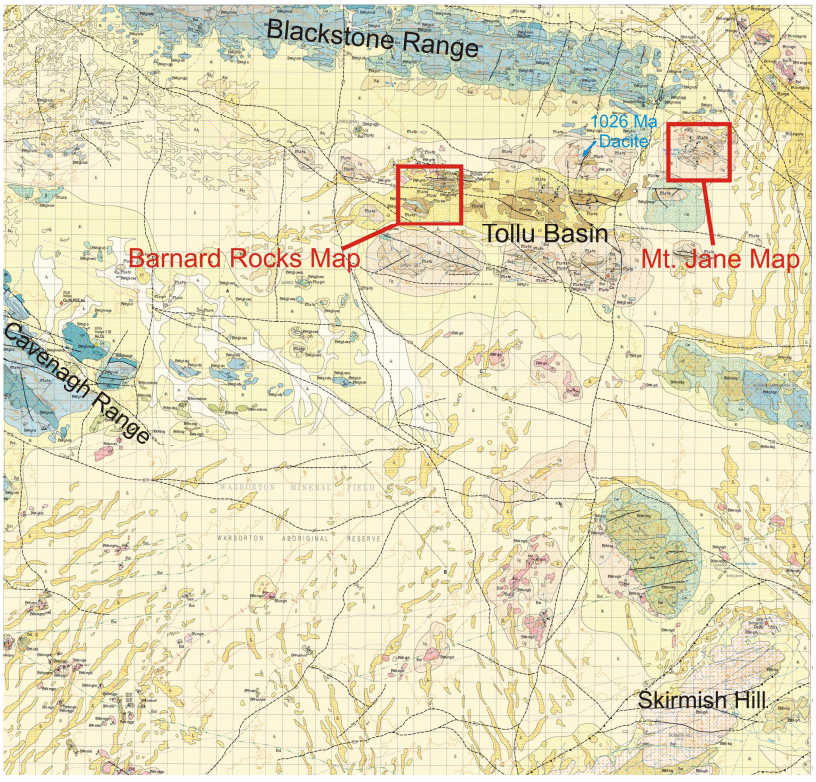

Mt Jane 1 :10 000 Geological Map

Figure 2

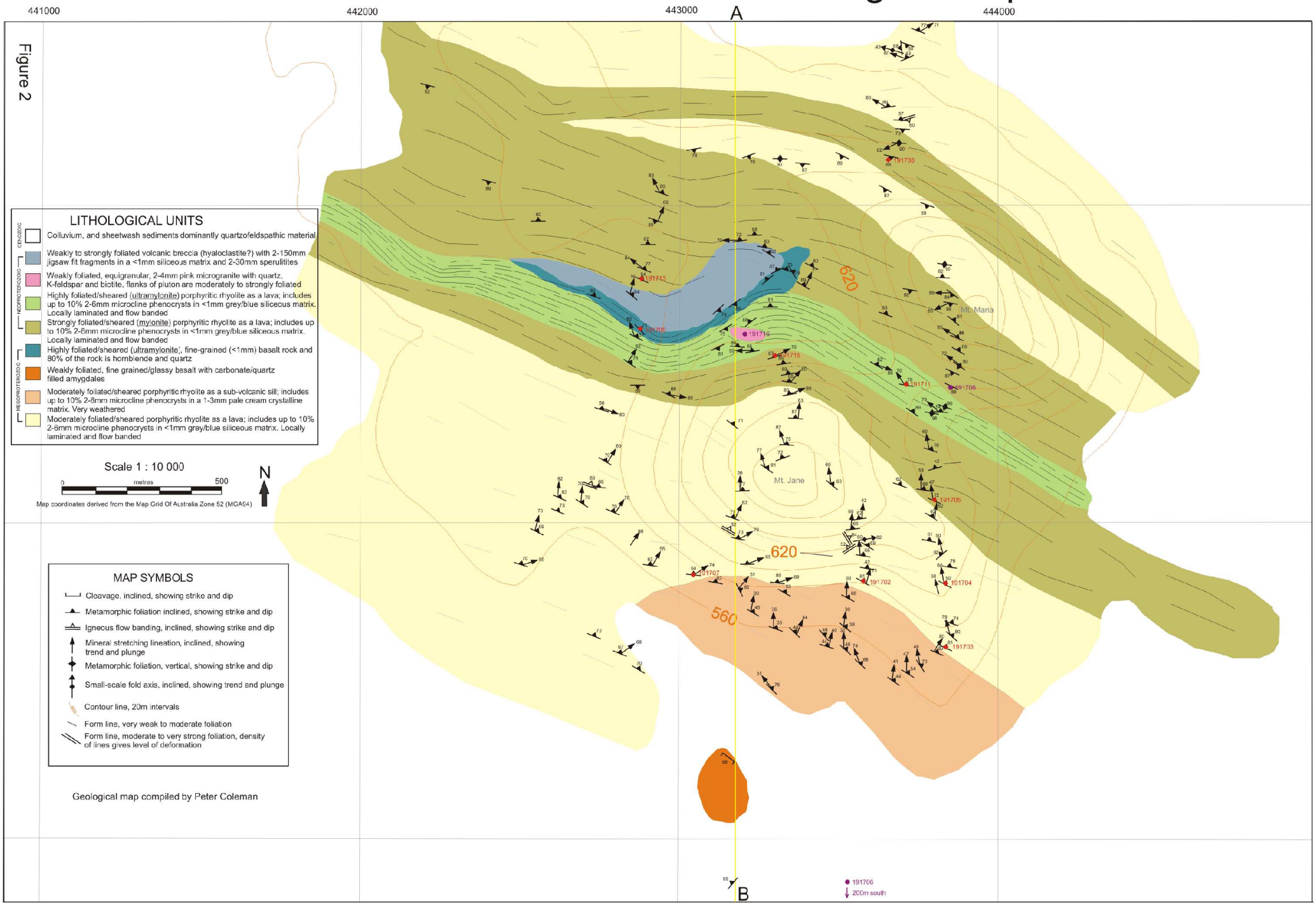

LITHOLOGICAL UNITS

CENOZOIC

Colluvium, and sheetwash sediments dominantly quartzofeldspathic material

NEOPROTEROZOIC

Weakly to strongly foliated volcanic breccia (hyaloclastite?) with 2-150mm jigsaw fit fragments in a <1mm siliceous matrix and 2-30mm spherulitites

Weakly foliated, equigranular, 2-4mm pink microgranite with quartz, K-feldspar and biotite, flanks of pluton are moderately to strongly foliated

Highly foliated/sheared (ultramylonite) porphyritic rhyolite as a lava; includes up to 10% 2-6mm microcline phenocrysts in <1mm grey/blue siliceous matrix. Locally laminated and flow banded

Strongly foliated/sheared (mylonite) porphyritic rhyolite as a lava; includes up to 10% 2-6mm microcline phenocrysts in <1mm grey/blue siliceous matrix. Locally laminated and flow banded

Highly foliated/sheared (ultramylonite), fine-grained (<1mm) basalt rock and 80% of the rock is hornblende and quartz

MESOPROTEROZOIC

Weakly foliated, fine grained/glassy basalt with carbonate/quartz filled amygdales

Moderately foliated/sheared porphyritic rhyolite as a sub-volcanic sill; includes up to 10% 2-8mm microcline phenocrysts in a 1-3mm pale cream crystalline matrix. Very weathered

Moderately foliated/sheared porphyritic rhyolite as a lava; includes up to 10% 2-6mm microcline phenocrysts in <1mm grey/blue siliceous matrix. Locally laminated and flow banded

Scale 1 : 10 000

0 metres 500

N

Map coordinates derived from the Map Grid Of Australia Zone 52 (MGA94)

MAP SYMBOLS

- Cleavage, inclined, showing strike and dip
- Metamorphic foliation inclined, showing strike and dip
- Igneous flow banding, inclined, showing strike and dip
- Mineral stretching lineation, inclined, showing trend and plunge
- Metamorphic foliation, vertical, showing strike and dip
- Small-scale fold axis, inclined, showing trend and plunge
- Contour line, 20m intervals
- Form line, very weak to moderate foliation
- Form line, moderate to very strong foliation, density of lines gives level of deformation

Geological map compiled by Peter Coleman

Figure 3

Mt Jane Geological Cross Section

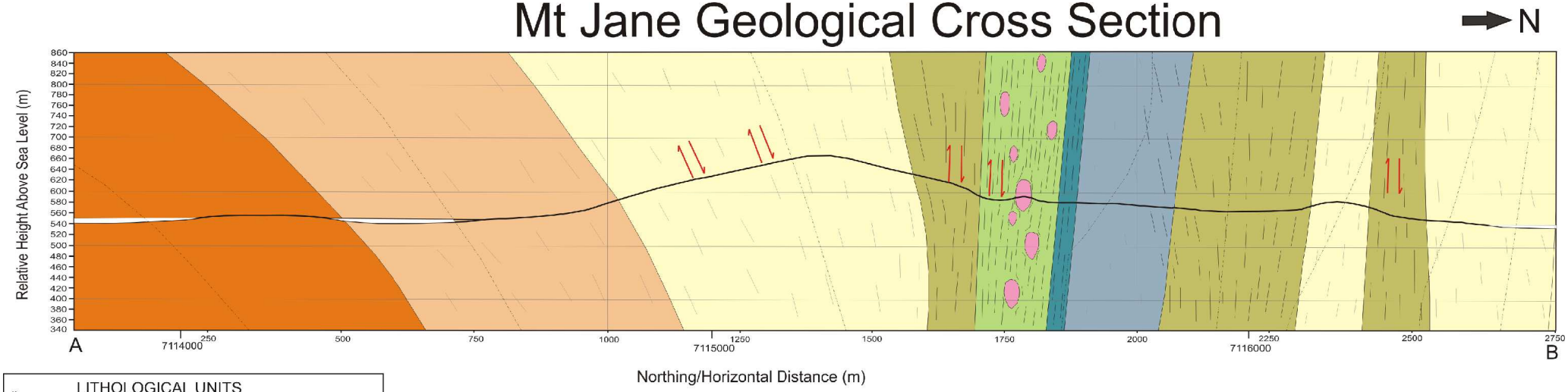

LITHOLOGICAL UNITS

CENOZOIC

- Colluvium, and sheetwash sediments dominantly quartzofeldspathic material

NEOPROTEROZOIC

- Weakly to strongly foliated volcanic breccia (hyaloclastite?) with 2-150mm jigsaw fit fragments in a <1mm siliceous matrix and 2-30mm sperulitites
- Weakly foliated, equigranular, 2-4mm pink microgranite with quartz, K-feldspar and biotite, flanks of pluton are moderately to strongly foliated
- Highly foliated/sheared (ultramylonite) porphyritic rhyolite as a lava; includes up to 10% 2-6mm microcline phenocrysts in <1mm grey/blue siliceous matrix. Locally laminated and flow banded
- Strongly foliated/sheared (mylonite) porphyritic rhyolite as a lava; includes up to 10% 2-6mm microcline phenocrysts in <1mm grey/blue siliceous matrix. Locally laminated and flow banded
- Highly foliated/sheared (ultramylonite), fine-grained (<1mm) basalt rock and 80% of the rock is hornblende and quartz

MESOPROTEROZOIC

- Weakly foliated, fine-grained/glassy basalt with quartz/carbonate filled amygdales.
- Moderately foliated/sheared porphyritic rhyolite as a sub-volcanic sill; includes up to 10% 2-6mm microcline phenocrysts in a 1-3mm pale cream crystalline matrix. Very weathered
- Moderately foliated/sheared porphyritic rhyolite as a lava; includes up to 10% 2-6mm microcline phenocrysts in <1mm grey/blue siliceous matrix. Locally laminated and flow banded

MAP SYMBOLS

- Lithological boundary between units
- Dip of igneous layering/flow-banding
- Form line, very weak to moderate foliation
- Form line, moderate to very strong foliation, density of lines gives level of deformation

Vertical / Horizontal Distance = 1

Compiled by Peter Coleman

Barnard Rocks Geological Map

Figure 4

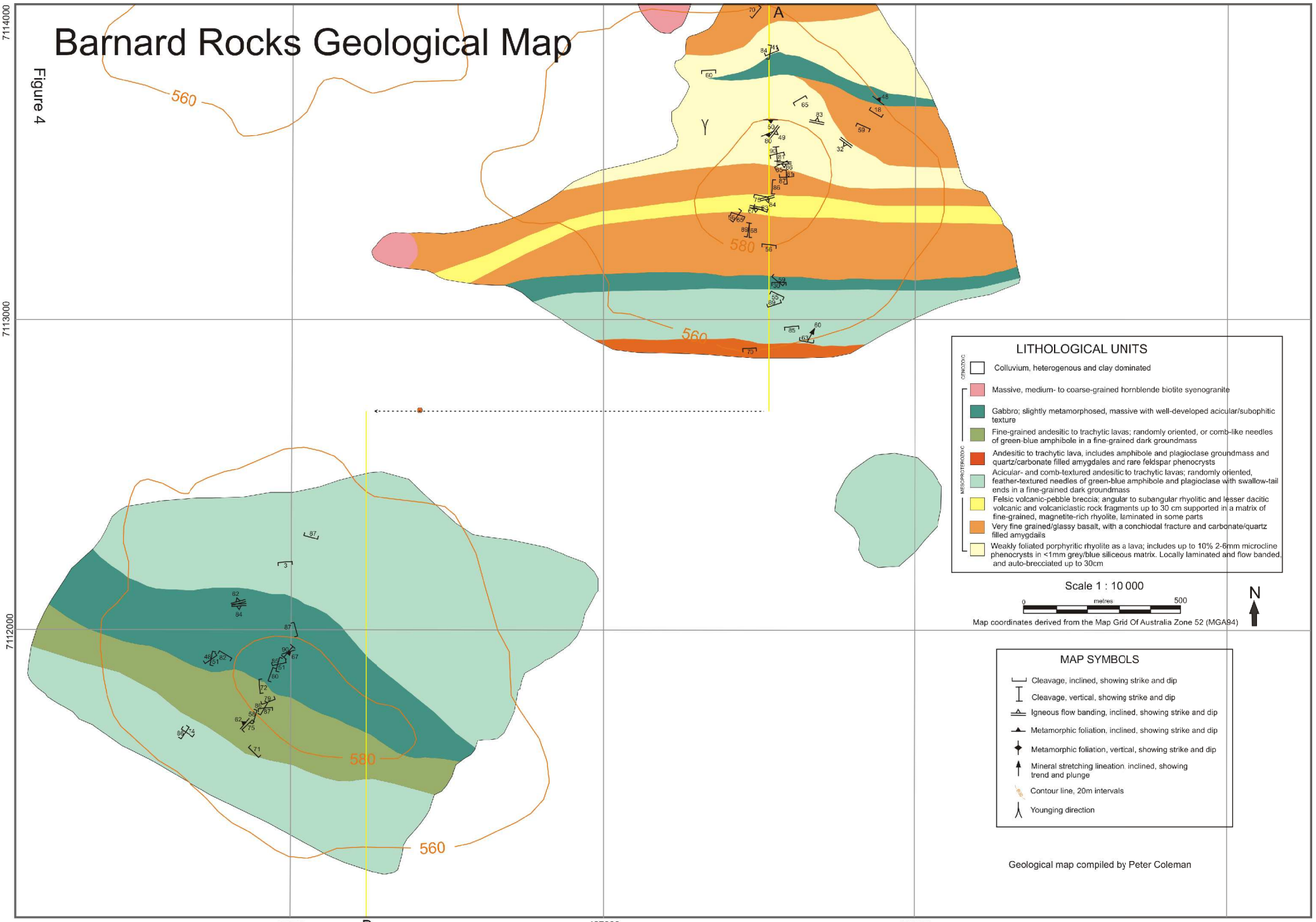

LITHOLOGICAL UNITS

CENOZOIC
- Colluvium, heterogenous and clay dominated

MESOPROTEROZOIC
- Massive, medium- to coarse-grained hornblende biotite syenogranite
- Gabbro; slightly metamorphosed, massive with well-developed acicular/subophitic texture
- Fine-grained andesitic to trachytic lavas; randomly oriented, or comb-like needles of green-blue amphibole in a fine-grained dark groundmass
- Andesitic to trachytic lava, includes amphibole and plagioclase groundmass and quartz/carbonate filled amygdales and rare feldspar phenocrysts
- Acicular- and comb-textured andesitic to trachytic lavas; randomly oriented, feather-textured needles of green-blue amphibole and plagioclase with swallow-tail ends in a fine-grained dark groundmass
- Felsic volcanic-pebble breccia; angular to subangular rhyolitic and lesser dacitic volcanic and volcaniclastic rock fragments up to 30 cm supported in a matrix of fine-grained, magnetite-rich rhyolite, laminated in some parts
- Very fine grained/glassy basalt, with a conchiodal fracture and carbonate/quartz filled amygdalis
- Weakly foliated porphyritic rhyolite as a lava; includes up to 10% 2-6mm microcline phenocrysts in <1mm grey/blue siliceous matrix. Locally laminated and flow banded, and auto-brecciated up to 30cm

Scale 1 : 10 000

0 metres 500

N

Map coordinates derived from the Map Grid Of Australia Zone 52 (MGA94)

MAP SYMBOLS

- Cleavage, inclined, showing strike and dip
- Cleavage, vertical, showing strike and dip
- Igneous flow banding, inclined, showing strike and dip
- Metamorphic foliation, inclined, showing strike and dip
- Metamorphic foliation, vertical, showing strike and dip
- Mineral stretching lineation inclined, showing trend and plunge
- Contour line, 20m intervals
- Younging direction

Geological map compiled by Peter Coleman

Figure 5

Barnard Rocks Geological Cross Section

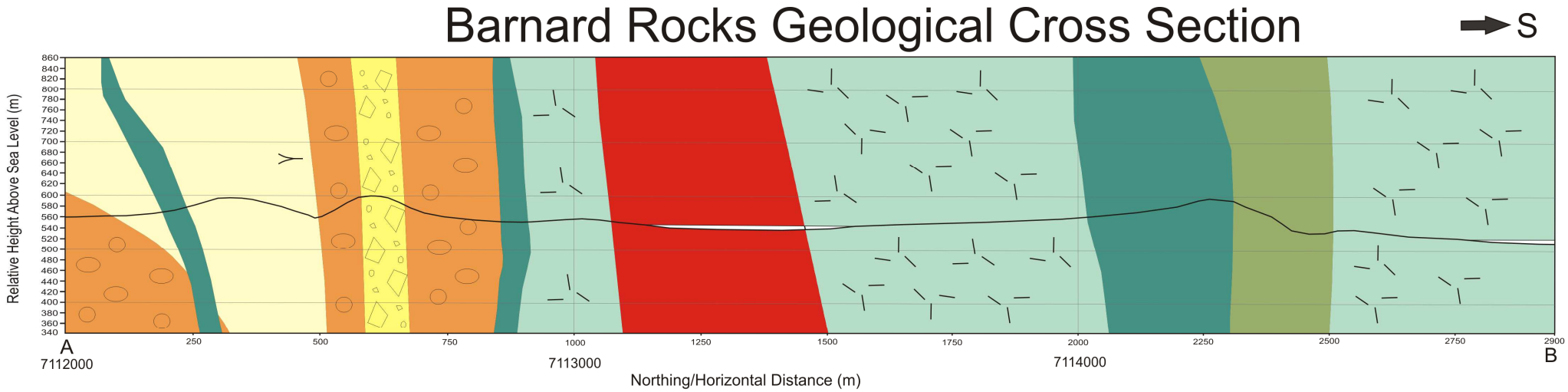

LITHOLOGICAL UNITS

CENOZOIC

- Colluvium, heterogenous and clay dominated

MESOPROTEROZOIC

- Massive, medium- to coarse-grained hornblende biotite syenogranite
- Gabbro; slightly metamorphosed, massive with well-developed acicular/subophitic texture
- Fine-grained andesitic to trachytic lavas; randomly oriented, or comb-like needles of green-blue amphibole in a fine-grained dark groundmass
- Very fine grained/glassy basalt, with a conchiodal fracture and carbonate/quartz filled amygdails
- Acicular- and comb-textured andesitic to trachytic lavas; randomly oriented, feather-textured needles of green-blue amphibole and plagioclase with swallow-tail ends in a fine-grained dark groundmass
- Felsic volcanic-pebble breccia; angular to subangular rhyolitic and lesser dacitic volcanic and volcaniclastic rock fragments up to 30 cm supported in a matrix of fine-grained, magnetite-rich rhyolite, laminated in some parts
- Andesitic to trachytic lava, includes amphibole and plagioclase groundmass and quartz/carbonate filled amygdales and rare feldspar phenocrysts
- Weakly foliated porphyritic rhyolite as a lava; includes up to 10% 2-6mm microcline phenocrysts in <1mm grey/blue siliceous matrix. Locally laminated and flow banded, and auto-brecciated up to 30cm

MAP SYMBOLS

- Lithological boundary between units
- Inferred lithological boundary
- Younging direction
- Topography

Vertical / Horizontal Distance = 1

Compiled by Peter Coleman

Figure 6(a) Lithological photos (b)

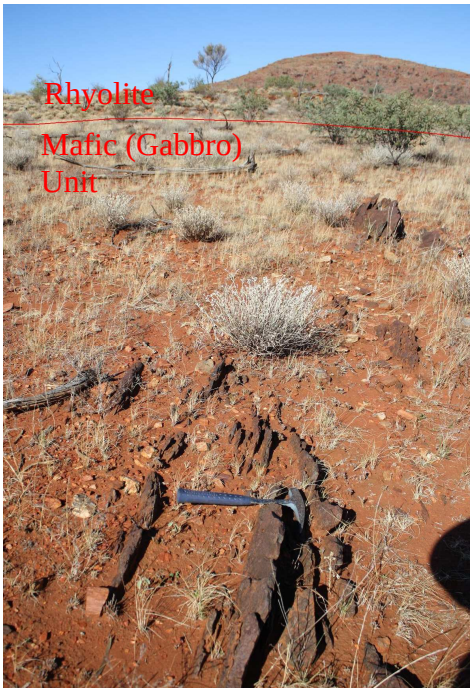

(c)

(d)

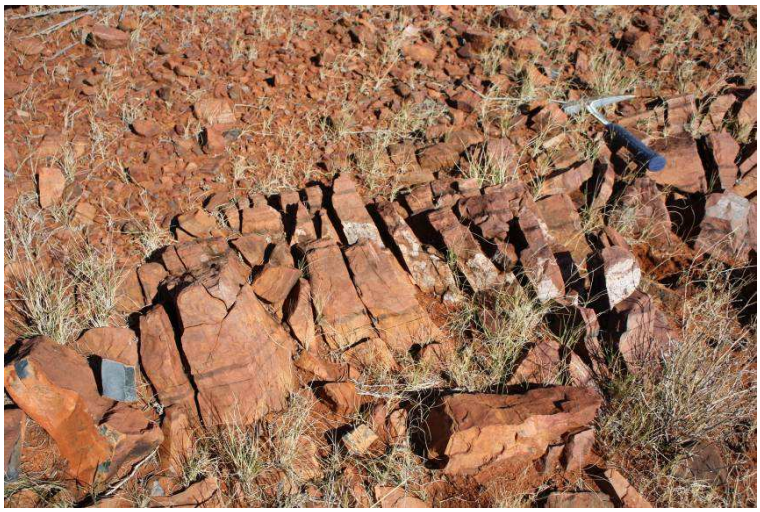

(e)

(f)

Figure 7(a) Structural photos (b)

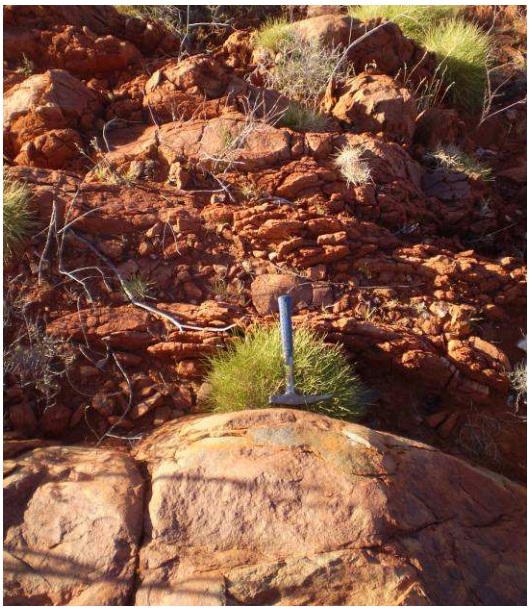

(c) (d)

(e)

Figure 8(a) Mount Jane lineations all data. Lineation plunge and trend

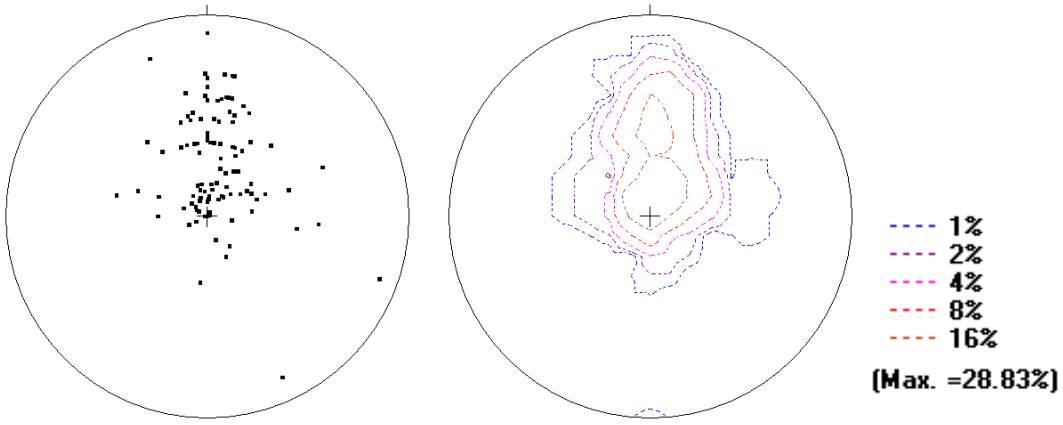

No. of Data = 111

(b) Mount Jane foliations all data. Poles to foliation strike and dip.

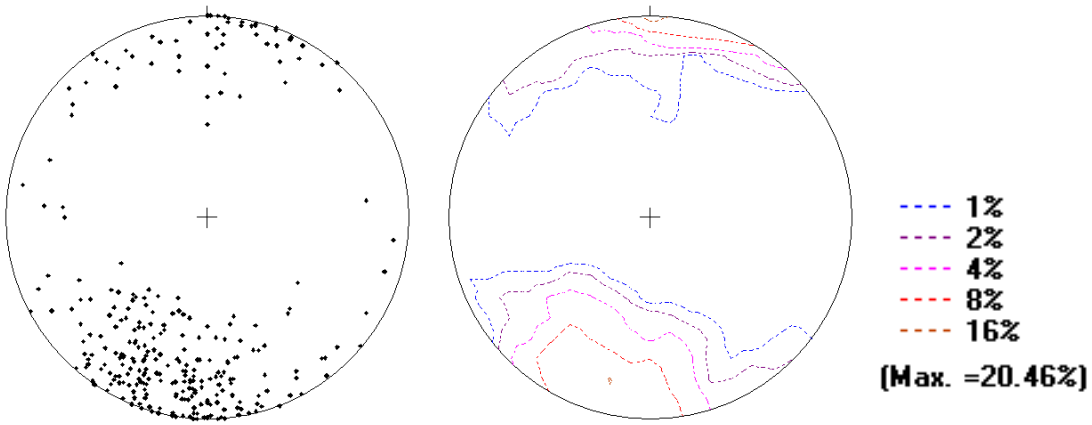

No. of Data = 303

(c) Stop 291, North Mount Jane, small scale (5m) fold. Poles to foliation strike and dip.

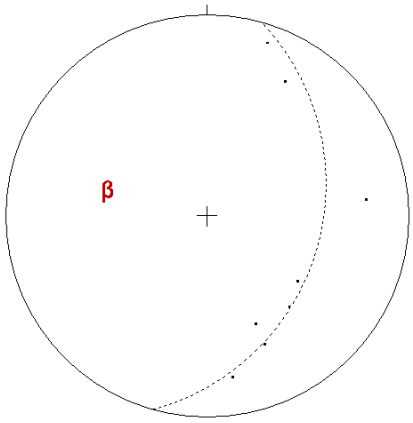

Calculated girdle: 43/106
Calculated beta axis: 47-286

No. of Data = 8

(d) Larger scale fold, stop 270-290 (North Mount Jane). Poles to foliation strike and dip.

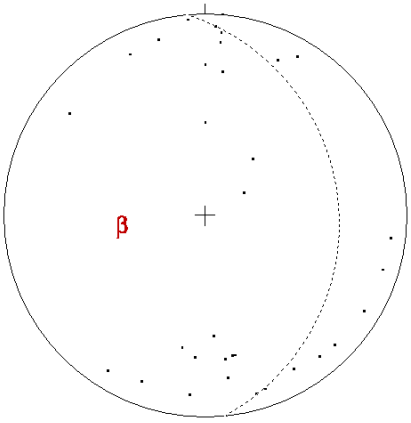

Calculated girdle: 34/084
Calculated beta axis: 56-264

No. of Data = 35

(e) Igneous flow banding all data, Mount Jane. Poles to strike and dip of layers.

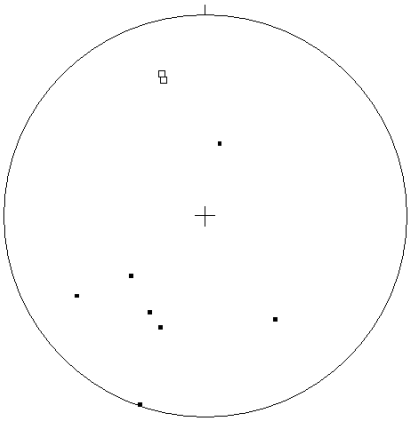

Open squares represent igneous flow banding north of the ultramylonite zone, Mount Jane
Smaller squares represent igneous flow banding south of the ultramylonite zone, Mount Jane

No. of Data = 9

(f) Barnard Rocks, fracture planes, all data. Poles to fracture strike and dip.

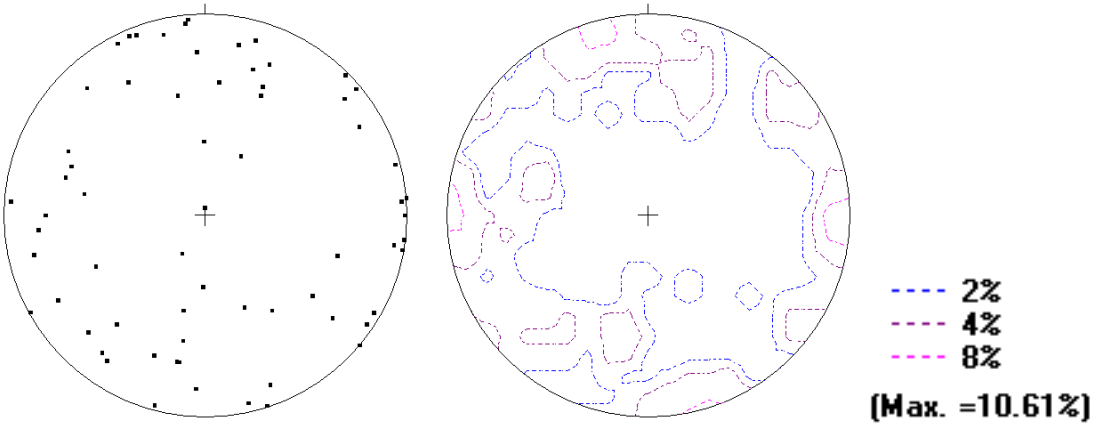

No. of Data = 71

(g) Barnard Rocks, fracture sets only. Poles to fracture strike and dip.

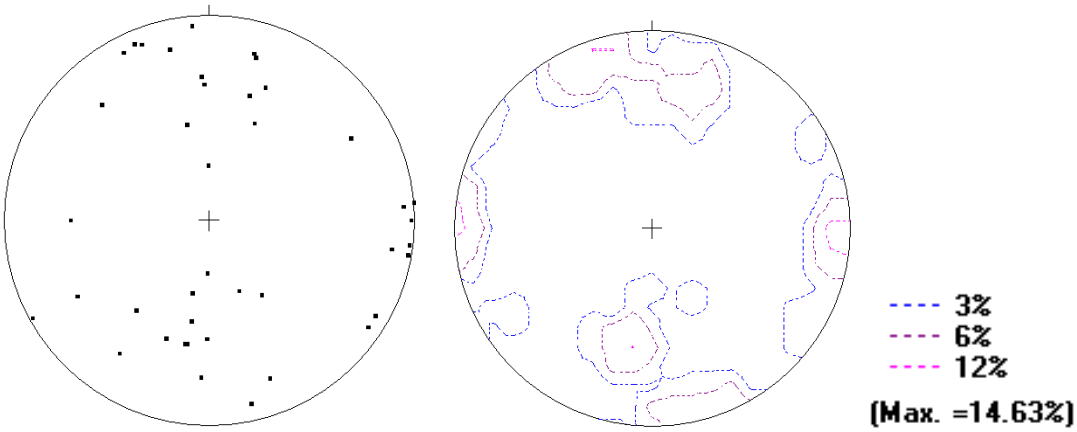

No of Data = 42

(h) Barnard Rocks, igneous flow banding, all data. Poles to strike and dip of beds.

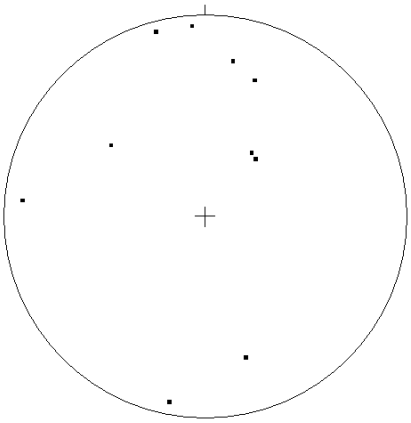

No of Data = 10

Figure 9(a)

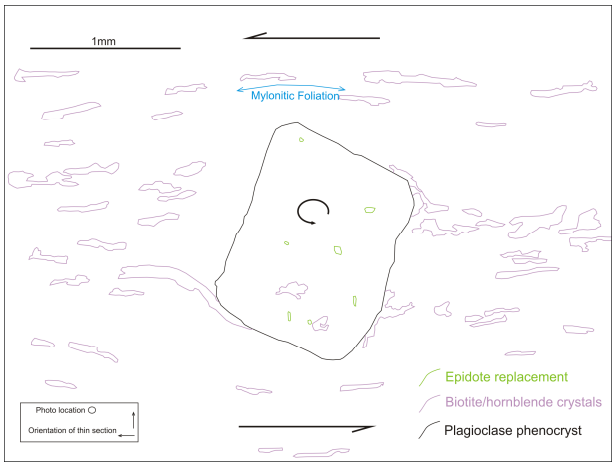
1mm
Mylonitic Foliation
Epidote replacement
Biotite/hornblende crystals
Plagioclase phenocryst
Photo location
Orientation of thin section

(b)

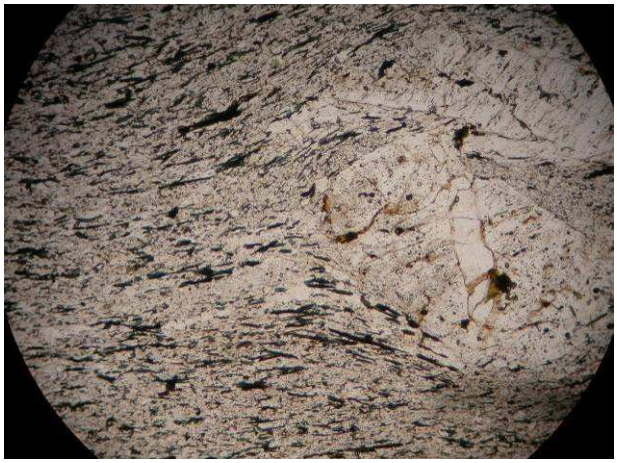

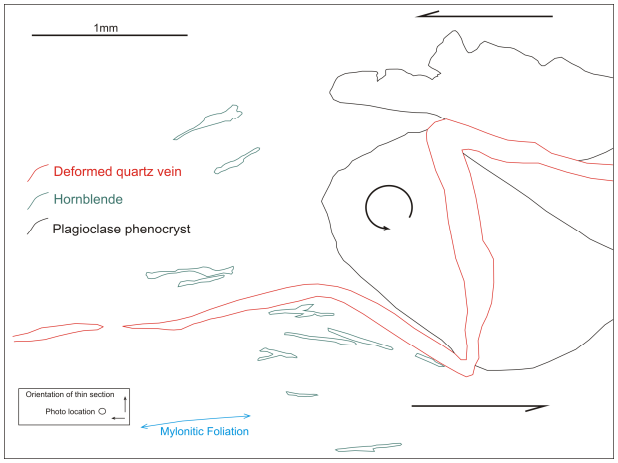
1mm
Deformed quartz vein
Hornblende
Plagioclase phenocryst
Orientation of thin section
Photo location
Mylonitic Foliation

(c)

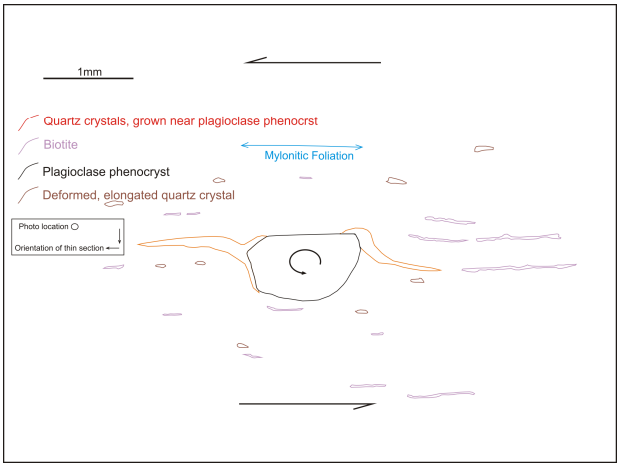
1mm
Quartz crystals, grown near plagioclase phenocrst
Biotite
Mylonitic Foliation
Plagioclase phenocryst
Deformed, elongated quartz crystal
Photo location
Orientation of thin section

(d)

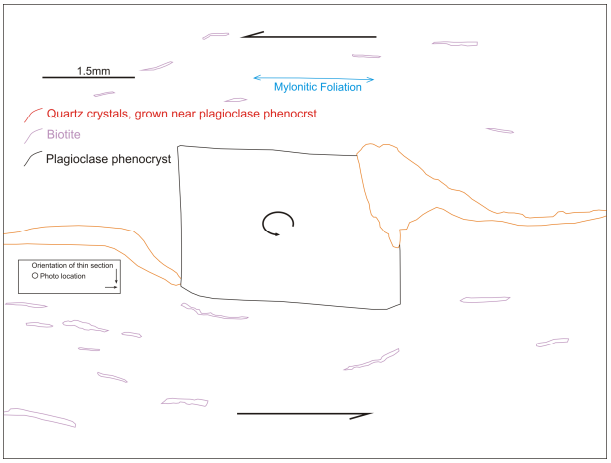
1.5mm
Mylonitic Foliation
Quartz crystals, grown near plagioclase phenocrst
Biotite
Plagioclase phenocryst
Orientation of thin section
O Photo location

(e)

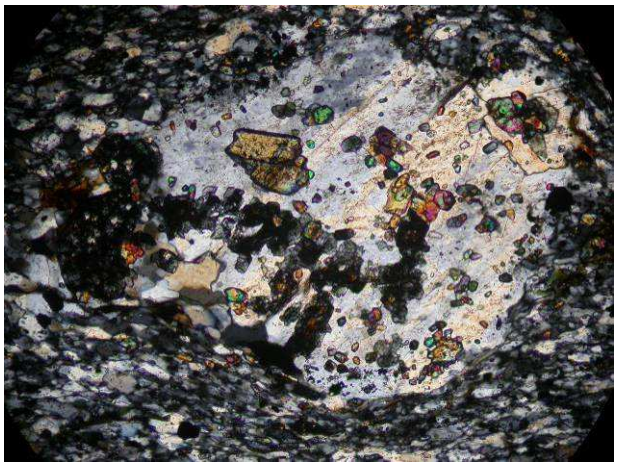

(f)

(g)

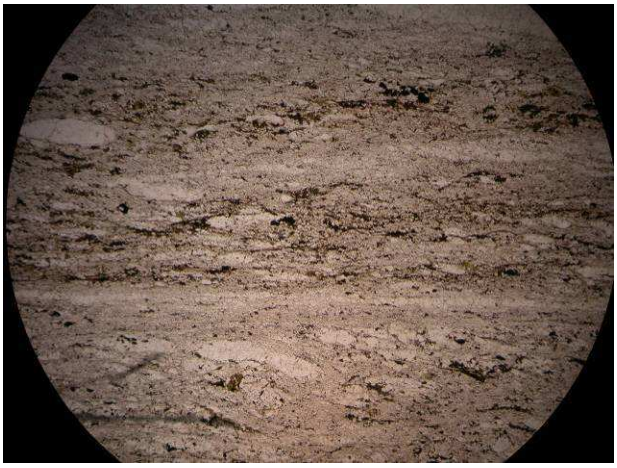

(h)

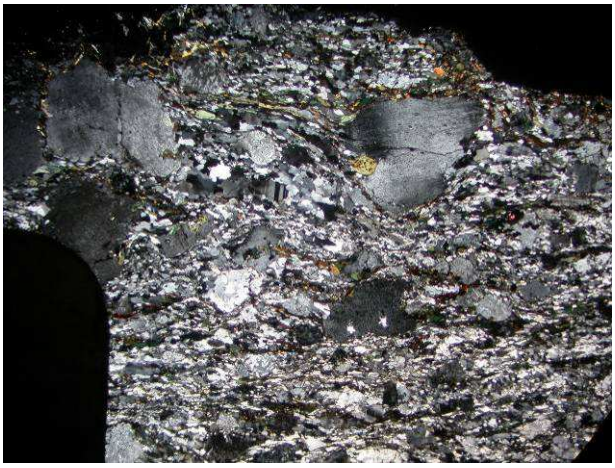

Figure 10(a)

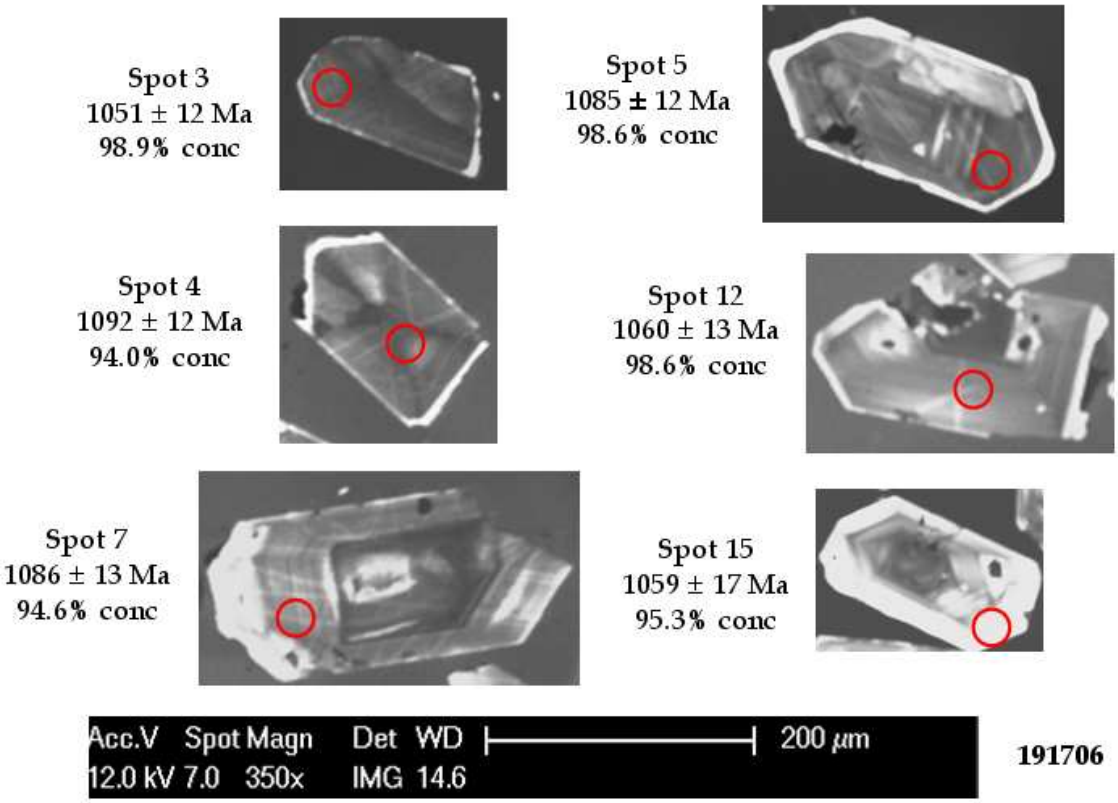
Spot 3
1051 ± 12 Ma
98.9% conc
Spot 5
1085 ± 12 Ma
98.6% conc
Spot 4
1092 ± 12 Ma
94.0% conc
Spot 12
1060 ± 13 Ma
98.6% conc
Spot 7
1086 ± 13 Ma
94.6% conc
Spot 15
1059 ± 17 Ma
95.3% conc
Acc.V Spot Magn Det WD 200 µm
12.0 kV 7.0 350x IMG 14.6
191706

(b)

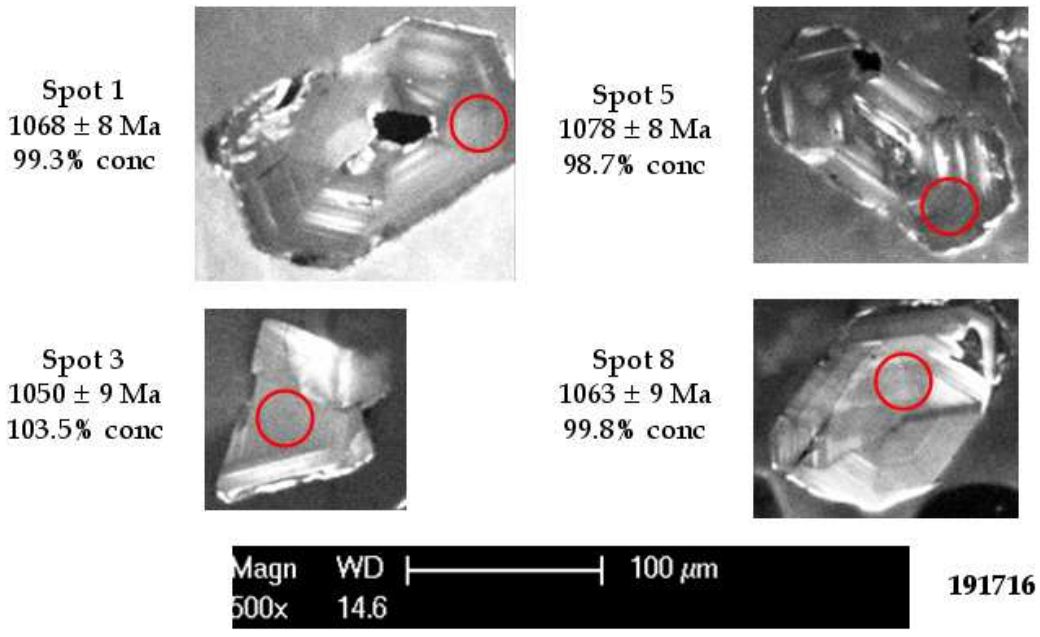
Spot 1
1068 ± 8 Ma
99.3% conc
Spot 5
1078 ± 8 Ma
98.7% conc
Spot 3
1050 ± 9 Ma
103.5% conc
Spot 8
1063 ± 9 Ma
99.8% conc
Magn WD 100 µm
500x 14.6
191716

(c)

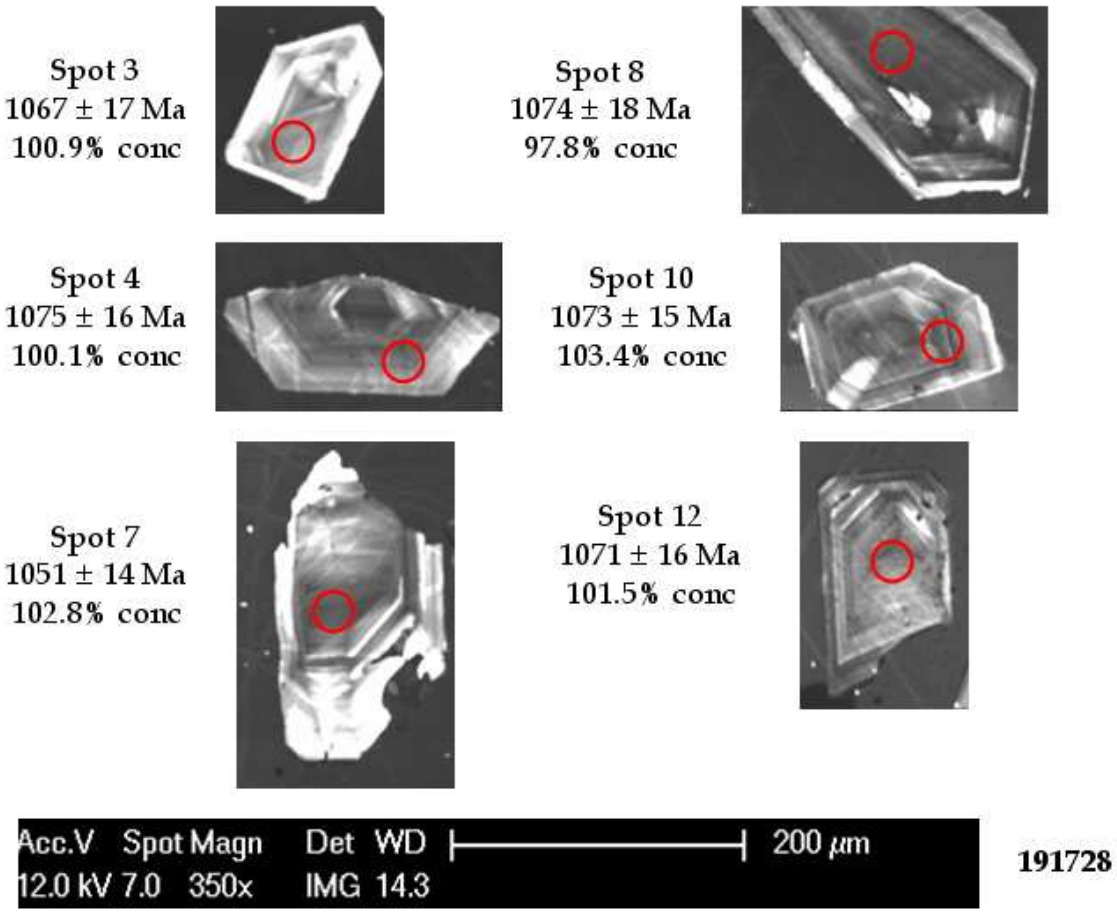
Spot 3
1067 ± 17 Ma
100.9% conc
Spot 8
1074 ± 18 Ma
97.8% conc
Spot 4
1075 ± 16 Ma
100.1% conc
Spot 10
1073 ± 15 Ma
103.4% conc
Spot 7
1051 ± 14 Ma
102.8% conc
Spot 12
1071 ± 16 Ma
101.5% conc
Acc.V Spot Magn Det WD 200 μm
12.0 kV 7.0 350x IMG 14.3
191728

Figure 11(a)

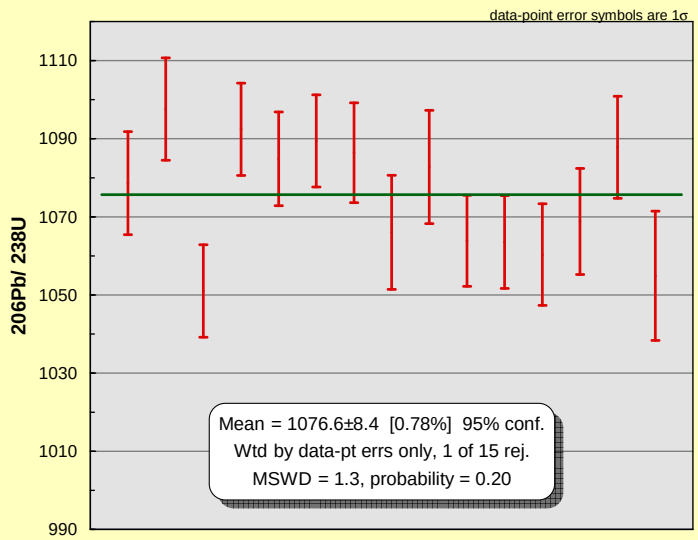

(b)

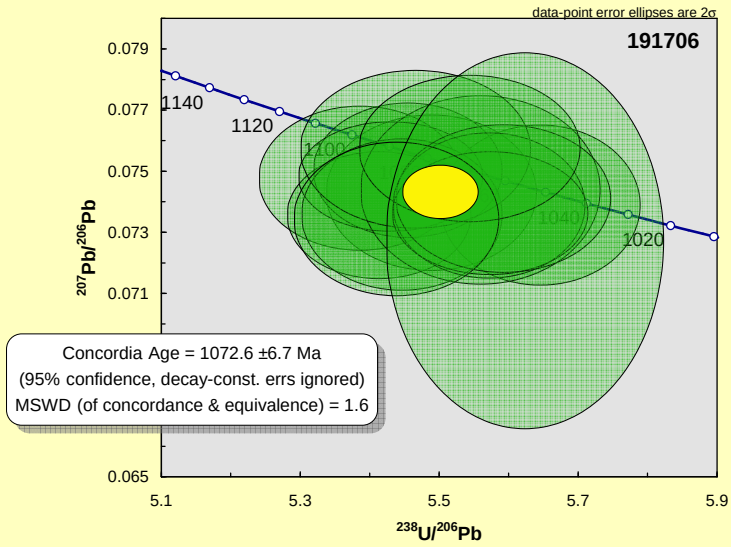

Figure 12(a)

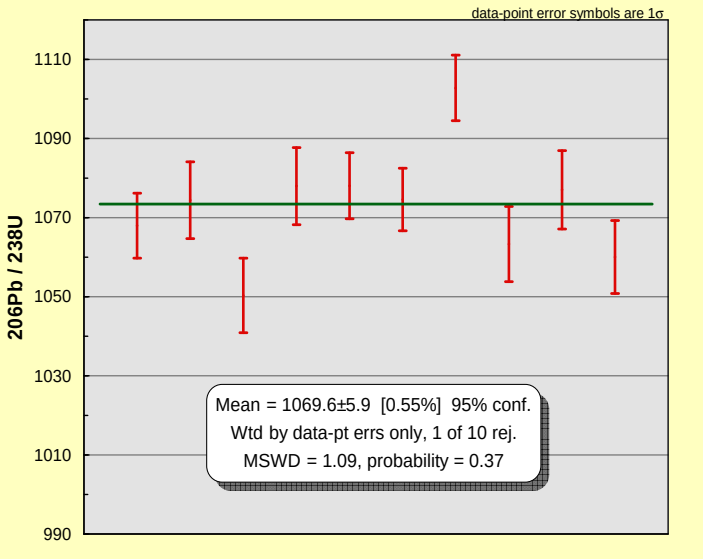

(b)

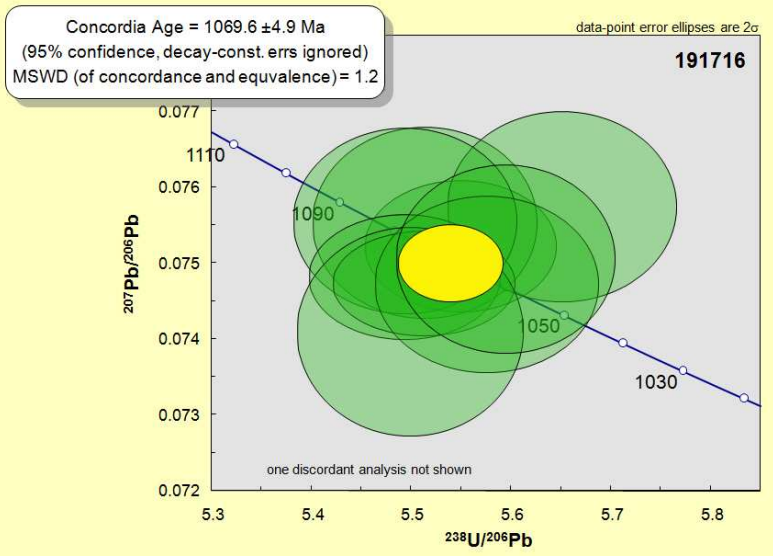

Figure 13(a) (b)

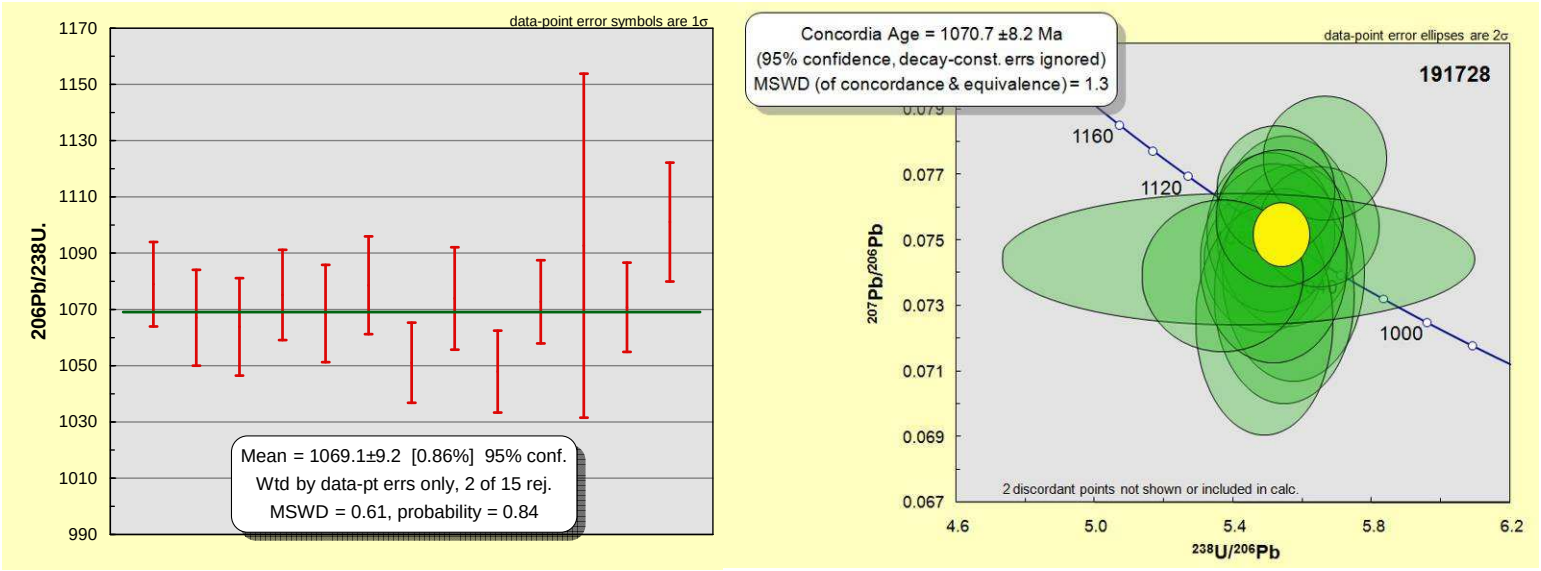
data-point error symbols are 1σ
206Pb/238U.
1170
1150
1130
1110
1090
1070
1050
1030
1010
990
Mean = 1069.1±9.2 [0.86%] 95% conf.
Wtd by data-pt errs only, 2 of 15 rej.
MSWD = 0.61, probability = 0.84
Concordia Age = 1070.7 ±8.2 Ma
(95% confidence, decay-const. errs ignored)
MSWD (of concordance & equivalence) = 1.3
data-point error ellipses are 2σ
191728
1160
1120
1000
0.077
0.075
0.073
0.071
0.069
0.067
207Pb/206Pb
2 discordant points not shown or included in calc.
4.6
5.0
5.4
5.8
6.2
238U/206Pb